



School of Chemistry

Aluminium-oxide terminations for diamond as a route to low work function surfaces and the application of the hierarchical method to diamond.

Daniel Field

This thesis is submitted in partial fulfilment of the requirements for the Honours Degree of MSci at the University of Bristol

Professor Paul May

Dr Neil Fox

Physical and theoretical

Abstract

Diamond has the potential to exhibit a negative electron affinity (NEA) and has potential applications as a low work function material in thermionic energy converters and electron amplifiers. One way of achieving a NEA is to create a metal-oxygen termination on the diamond. Valuable insights into the electronic properties of materials of solids can be gained by modelling their electronic structure using wavefunction theory. The experimental aspect of this project was to fabricate a low work function diamond surface by the formation of an aluminium-oxygen termination and the theoretical aspect was focused on applying the hierarchical method to predict the band gap of diamond.

Polycrystalline diamond films were grown, oxygen terminated by exposure to oxygen plasma and aluminium was deposited in a thick layer by evaporation before being acid etched to give an atomically thin aluminium coating. The samples were characterised by Raman spectroscopy, energy dispersive X-ray spectroscopy, scanning electron microscopy, X-ray photoelectron spectroscopy (XPS), and thermionic emission measurements. Characterisation of the modified diamond indicated that aluminium deposition was not homogenous and that less than a monolayer of aluminium remained after etching. Analysis of XPS peaks indicated that this aluminium was chemically bound to the diamond surface. Heating the aluminium coated diamond prior to etching increased the quantity of aluminium retained and caused the apparent formation of aluminium carbide. Thermionic emission experiments showed no electron emission from the modified diamond, even at temperatures as high as 600°C, indicating that the attempt to produce a low work function surface with a NEA was unsuccessful.

In applying the hierarchical method, diamond clusters were built using GaussView and energy calculations performed using density functional theory (DFT) with the B3LYP functional using the Turbomole package and the def-SVP basis set. Total energies of neutral, anionic, and cationic clusters were calculated and the energy per bulk atom of the anion minus that of the cation were used as an estimate for the band gap. The resulting band gaps calculated were not comparable with experimental or computational values. Additionally, the calculated energies per bulk atom did not converge with increasing cluster size. This lack of convergence was ascribed to a lack of a hierarchical structure in the diamond clusters. When a systematic method of growth was uncovered, the energies per bulk atom of neutral clusters converged within 0.002 eV, underlying the importance of the hierarchy. However, this method of systematic growth caused a large increase in the number of atoms per cluster. This large increase prevented application of wavefunction theory due to the large computational cost entailed.

Acknowledgements

My thanks go to my supervisor Professor Paul May as well as to my second assessor Dr Neil Fox for their guidance throughout the course of my project. Also to the Bristol university diamond group for all their help and particularly to Mr Michael James. Without his day-to-day help, I would not have achieved much. I would also like to thank Professor Neil Allan, Dr David Tew, and Dr Peter Bygrave for supervising the theoretical aspect of my project and having the patience with me as I took my first steps into computational chemistry. Finally, I would also like to thank my mother for her patience and help in making sense of my ramblings.

Contents

1 Introduction	5
1.1 Project Overview.....	5
1.2 Diamond.....	8
1.2.1 General Functionalisation and Doping of Diamond.....	11
1.2.2 Oxygen terminations.....	13
1.2.3 Diamond as a Thermionic Emitter and the Negative Electron Affinity.....	14
1.3 Theoretical Concepts	25
1.3.1 The Hierarchical Method	26
1.4 Project Objectives	27
2 Experimental Materials and Methods	28
2.1 Materials	28
2.2 Chemical Vapour Deposition (CVD)	28
2.2.1 Substrate preparation.....	28
2.2.2 Undoped Hot-filament CVD	28
2.2.3 Nitrogen-doped Microwave Plasma CVD.....	29
2.4 Raman spectroscopy.....	30
2.5 Scanning electron microscopy (SEM).....	30
2.6 Energy-dispersive X-ray Spectroscopy (EDX)	31
2.3 Surface derivatisation	31
2.3.1 Oxygen Termination.....	31
2.3.2 Hydrogen Termination.....	32
2.3.3 Aluminium Deposition and Etching	32
2.6 X-ray Photoelectron Spectroscopy	33
2.7 Thermionic Emission Measurements.....	33
3 Results and Discussion	35
3.1 Development of an Aluminium-Oxygen Termination of Diamond.....	37
3.2 Thermionic Emission	49
3.3 Computational results.....	54
4 Conclusions and Further Work	59
5 References	63

1 Introduction

1.1 Project Overview

Society's reliance on polluting, non-renewable fuels, such as oil and gas, is unsustainable. Not only will such fuels run out – current estimates suggest that coal deposits will be exhausted by 2088¹ – their use is also having a disastrous effect on the world around us. Carbon emissions are contributing to climate change which is now posing a real threat to our society²⁻⁴ and is already impacting on our weather^{5,6}. Other pollutants released from burning fossil fuels are impacting on the population's health and well-being⁷⁻¹⁰ and all of these effects will only intensify if there is no change in how our energy is produced. There is an urgent need for renewable and clean energy sources to address this. Over the past few years the field of photovoltaics has received a lot of attention as one solution to this problem¹¹⁻¹⁴ but another option, which has received less attention, is the use of thermionic energy converters (TECs) to harness the sun's energy.

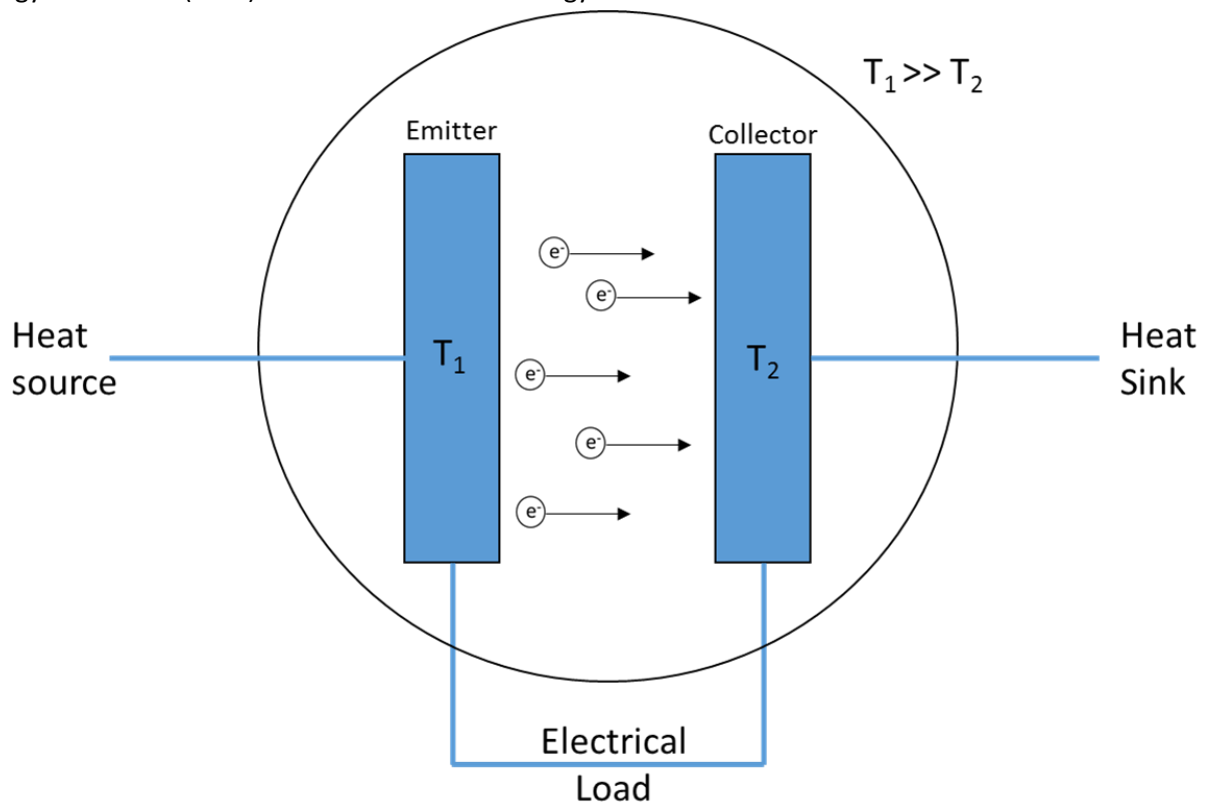


Figure 1: A thermionic energy converter

These devices harness the phenomenon of thermionic emission, *i.e.* the ejection of charge carriers from a material when thermally excited, to produce an electrical current^{15,16}. Thermionic emission is determined by the Richardson-Dushman equation,

$$J = A_G T^2 e^{-\phi/kT}, \quad (1)$$

where J is the emission current density, T is the temperature of the material, φ is the work function of the material, k is the Boltzmann constant, and A_G is a parameter given by

$$A_G = \lambda_B A_0, \quad (2)$$

where λ_B is a material-specific constant and A_0 is a universal constant^{17,18}.

In thermionic energy converters, two electrodes with a gap between them are connected to a circuit. One of these electrodes, the emitter, is heated above the emission temperature ($kT > \varphi$) causing thermionic emission. The electrons emitted are then collected by the other electrode (the collector), which is attached to a heat sink (Figure 1). The net flow of electrons between the two electrodes is sustained by the temperature gradient as electrons which reach the cooled collector electrode no longer have the necessary thermal energy for thermionic emission to occur. As electrons leave the emitter electrode and reach the collector electrode the result is a build-up of positive and negative charge, respectively and, hence, the generation of a potential difference and a current between the two electrodes. Evidently, having a low work function, thermally stable material is a necessity for this technology to provide a source of renewable energy, utilising either solar heat or waste heat from an industrial process.

In early TEC devices, the inter-electrode gap was under high vacuum. However, the main problem with TECs using an evacuated inter-electrode gap is the space-charge effect (Figure 2). As mentioned earlier, the emitter electrode builds up a positive charge whilst a negative charge builds up on the collector electrode. This results in a cloud of electrons residing above the surface of the emitter electrode which are attracted to the positive charge on the emitter and repelled by the negative charge on the collector. This layer of electrons produces electrical fields which repel subsequent electrons, slowing them down and even reflecting them back to the emitter. This results in an increase in the thermal energy required for electron emission, reducing the current generated. This space-charge effect makes vacuum TECs very inefficient.

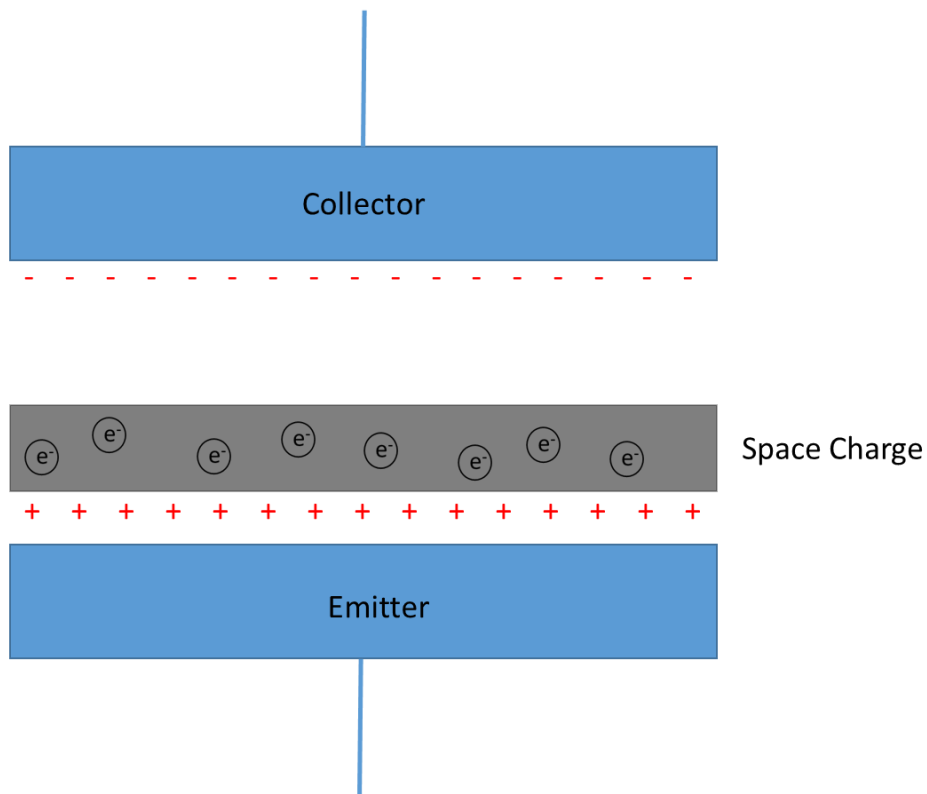


Figure 2: The space-charge effect in a TEC.

To combat this problem, vapour TECs were developed. These devices use vaporised positive ions, usually caesium ions, which neutralise the space charge and reduce the space charge effect. Such devices can still suffer from space-charge if there are not enough positive ions to neutralise the space charge. Additionally, they can be affected by unfavourable elastic collisions between emitted electrons and the positive ions.

Another method to overcome the space-charge effect is to place the two electrodes close together. This reduces the distance the electrons need to travel and so minimises the effect of space charging. The most substantial drawback with such devices is their need for electrodes manufactured from thermally stable, low work function materials ^{15,16}.

Other applications of low work function materials include those that require a high electron yield. For instance electron amplifiers in devices such as photomultipliers ¹⁹, ultra-high-power free-electron lasers ^{20,21}, and energy-recovery light sources (used for the production of x-rays) ^{22,23} and other such devices that require high-average current, high-brightness electron beams.

1.2 Diamond

Diamond is the hardest, stiffest and least compressible material known, as well as being very chemically inert and having the highest thermal conductivity of any material at room temperature and pressure^{24,25}. It has a face-centred cubic lattice with a unit cell (Figure 3), *i.e.* the smallest group of atoms that can reproduce the crystal lattice by translation alone, and a lattice parameter reported between 3.5 and 4.0 Å^{26,27}. There are three crystal planes commonly seen in diamond (Figure 4) (100), (110), and (111).

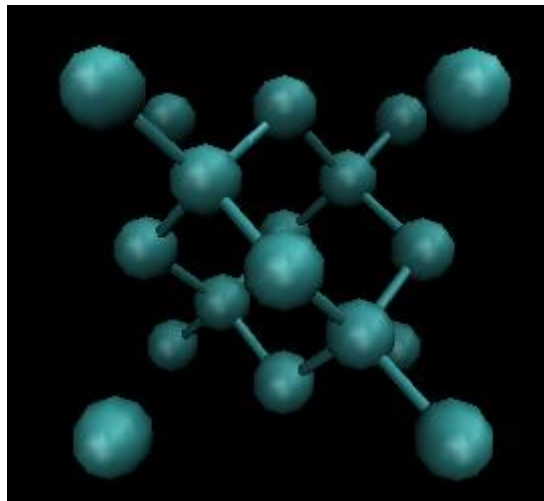


Figure 3: Diamond unit cell.

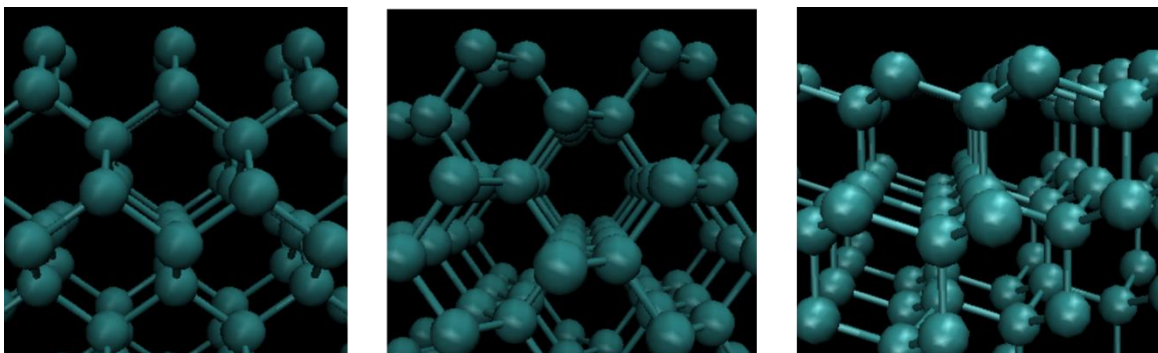


Figure 4: The different crystal planes of diamond from left to right (100), (110), and (111).

Producing synthetic diamond has always been of interest, partly because of its value as a gemstone used in jewellery, but also because of its industrial value, arising from its unique physical properties. The first synthetic diamonds were produced using the high temperature high-pressure (HPHT) method. This method attempts to replicate the conditions that produce natural diamond within the Earth's crust. A source of carbon (often graphite powder) is put under pressure (5-6.5 GPa) using hydraulic presses and then heated to between 1300-1700°C²⁸. The graphite powder is dissolved in a

molten transition-metal catalyst which carries the carbon to a diamond seed onto which it precipitates. This results in the formation of single-crystal diamonds in the size range of several hundred micrometres²⁴. It is also possible to carry this process out with non-metal catalysts and a variety of hydrocarbons as a carbon source rather than graphite^{24,29}.

Another technique for synthesising diamond is chemical vapour deposition (CVD) which results in the growth of a film of diamond onto a diamond or non-diamond substrate. There are a variety of different types of diamond film which can be produced using CVD: single crystal diamond (SCD), microcrystalline diamond (MCD), nanocrystalline diamond (NCD) and ultrananocrystalline diamond (UNCD). All of these types are produced by a gas-phase reaction generally between hydrogen and a hydrocarbon. The gases are activated, either thermally (hot filament CVD), by plasma (dc plasma and microwave CVD³⁰) or using combustion (torch CVD³¹)³². This process occurs above a substrate which must be heated to around 700°C in order to prevent the formation of amorphous carbon²⁵.

SCD is grown onto high quality HPHT or natural gemstone and results in the growth of a film of a single phase of crystal³². On the other hand, MCD, NCD and UNCD can all be grown on non-diamond substrates and have an irregular, polycrystalline growth. MCD has grain sizes between 1 µm and 1 mm and NCD has smaller grains ranging from 10 nm to a few hundred nm in size. UNCD is formed of even smaller grains (< 5 nm) and the diamond crystals are embedded into a sp² carbon matrix³². The type of diamond grown during CVD is controlled by the ratio of gases, the type of CVD used, as well as growth time and how the substrate is prepared for deposition³².

One of the limiting factors of CVD is the choice of substrates. These must have a high melting point to survive the harsh conditions in a CVD reactor as well as mirroring the thermal expansion of diamond to prevent cracking and delamination upon cooling³¹. Additionally, non-diamond substrates need to be able to form a thin layer of carbide for the diamond to deposit on to. However, the substrate material cannot have too great an affinity for carbon otherwise the diamond will dissolve into the substrate and form a thick carbide. Usually the substrate used is either diamond itself or silicon²⁵ seeded with diamond^{32,33} although some transition metals, such as molybdenum, can also be used³⁴. Other issues with diamond CVD include a slow growth rate, problems with creating large-area single-

ring closure occurs, propagating the diamond structure. Additionally, atomic hydrogen etches sp^2 carbon much faster than sp^3 which promotes the growth of diamond over graphite^{32, 37, 38}.

The (100) and (111) surfaces are the most commonly found in CVD grown diamond and reconstruct to give a dimerized chain like (2×1) surface (known as a Pandey chain) and a dimer surface respectively^{39,40}.

1.2.1 General Functionalisation and Doping of Diamond

Diamond is usually an insulator but can be doped using boron to produce a p-type semiconductor. This occurs in nature when boron defects give type IIb diamond²⁴ and can also be achieved during CVD diamond growth by including a source of boron (*e.g.* diborane) in the gas reaction mixture⁴¹. In p-type semiconductors the dopant atoms substitute for carbon into the lattice and act as ‘acceptors’, *i.e.* they have fewer electrons than carbon. This results in an extra electronic state that is slightly higher in energy than the valence band maximum (VBM) (Figure 5). It is easier to thermally excite electrons from the valence band into this level, which in turn results in positively charged ‘holes’ in the valence band. These holes can move throughout the material and produce a current when an electrical field is applied, *i.e.* the material has become an electrical conductor.

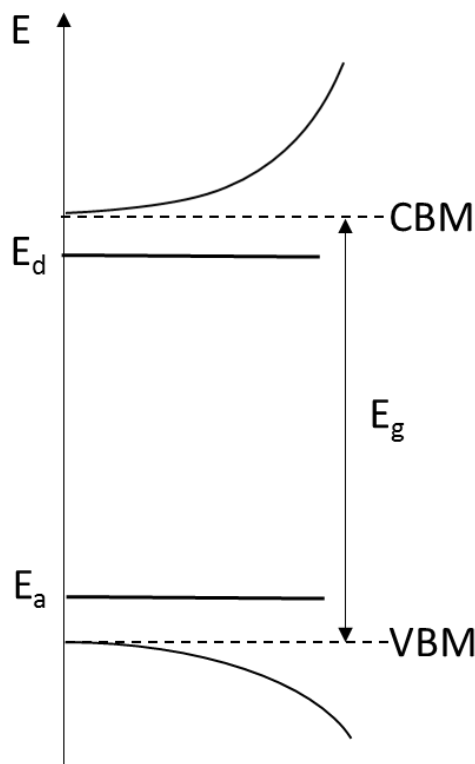


Figure 5: A schematic diagram of the positions of energy levels introduced by p-type (E_a) and n-type (E_d) dopants relative to the band gap (E_g), the valence band maximum (VBM) and the conduction band minimum (CBM).

In general, it is possible to introduce a different kind of semiconductivity, n-type, by the introduction of other kinds of dopants. These atoms have a higher number of valence electrons than carbon. When these dopants substitute into the native lattice, the extra electrons are donated to the lattice and introduce an additional energy level below the conduction band minimum (CBM) (Figure 5). These electrons are easily excited into the conduction band where they are free to act as charge carriers. Nitrogen was an early candidate for n-type doping in diamond considering that it is a light group five element but the donor level generated is too low in energy. This means the energy gap between the donor level and CBM is too large for nitrogen doped diamond to be conductive at room temperature. Calculations performed on lithium-doped diamond predicted it to create a donor level but this has not been confirmed experimentally probably due to issues in incorporating the lithium atoms into the diamond lattice. Using phosphorus as a dopant does give an n-type semiconductor when incorporated into the (111) surfaces but its electrical properties are too poor to be used in electrical devices⁴². As more complicated devices require a p-n junction, the inability to develop functional n-type semiconductivity in diamond means its use in electronics is currently limited to simple p-type devices, such as sensors and detectors⁴³.

As well as doping diamond, it is possible to chemically modify its surface utilising the 'dangling bond' mentioned above, for instance, organic molecules can be covalently bonded to the diamond surface using a variety of different methods. Two ways of doing this are by the photochemical reaction of alkenes to H-terminated diamond, or by the reduction of diazonium salts onto a H- or OH-terminated boron-doped diamond electrode. By bonding a primary amine to the diamond it is possible to subsequently bond thiol-modified DNA, enzymes and other proteins to the diamond surface⁴⁴. This, combined with our ability to make diamond a conducting material, leads to the exciting possibility of using diamond as transducer material in biosensors^{44,45}. Another method for functionalisation diamond surfaces is the esterification reaction between oxidised diamond and a variety of different organic molecules. Through such reactions, a whole range of new functionality can be introduced to the diamond surface - this offers another method for the tethering of DNA. It is also possible to silanise the surface of oxidised diamond. This can be useful in giving barrier properties, for example adsorbed perfluorodecyl trichlorosilane almost entirely blocks the electron transfer from adsorbed compounds⁴⁶.

1.2.2 Oxygen terminations

Different reaction methods with oxygen can lead to different geometries and types of oxygen termination. The two most stable geometries are a ketone-style C=O normal to the surface of the diamond or an ether-style linkage between two surface carbons (Figure 6), with hydroxyl terminations also having been observed⁴⁷⁻⁴⁹. A comparison of electrochemical, oxygen plasma and photochemical oxygen termination methods on polycrystalline diamond films undertaken by Wang *et al.* resulted in a mixture of oxygen terminations being formed, although the proportions differed depending on the method of oxygen termination⁴⁸. It seems likely that mixtures were formed due to the diamond being polycrystalline; different crystal planes have different structures and will favour different oxygen geometries to reduce steric clashes. Electrochemical oxidation mainly resulted in formation of hydroxyl groups whilst exposure to oxygen plasma predominantly resulted in ether-type terminations. A photochemical oxidation also largely resulted in formation of ether-type terminations, although a greater proportion of hydroxyl groups were also formed. In all cases there was little evidence for the presence of the ketone oxidation, an observation consistent with DFT calculations which suggest that on a (100)-(2 × 1):O reconstructed diamond surface the ketone arrangement is much less stable than the ether geometry, with no energy barrier between the two³⁹. It has also been observed that acid washing results in oxygen terminations, and although their exact nature has yet to be defined, their properties differ from samples oxygenated by plasma exposure, for instance how they interact with further adsorbates^{50,51}.

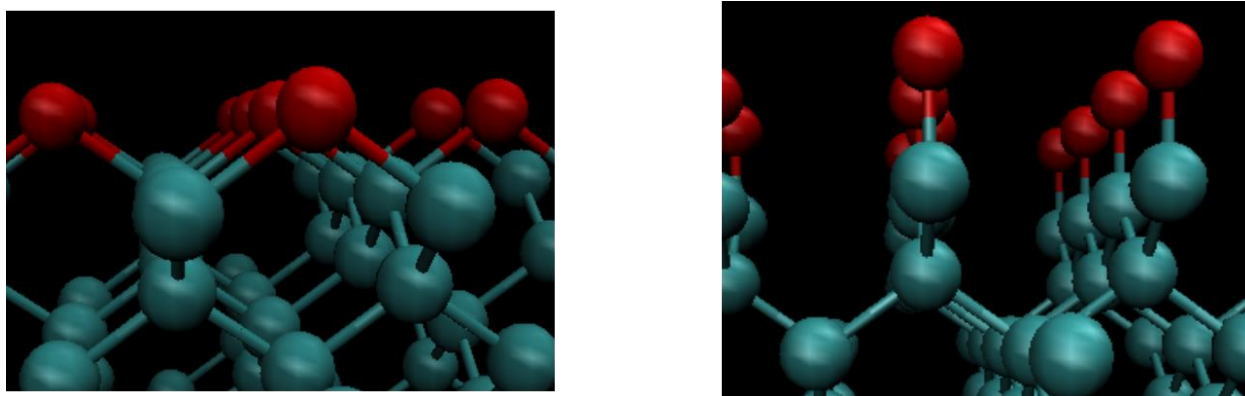


Figure 6: Ether bridging oxygen termination (left) and carbonyl oxygen termination (right) on a (100) diamond surface.

1.2.3 Diamond as a Thermionic Emitter and the Negative Electron Affinity

By exposing a diamond surface to hydrogen plasma, it is possible to produce a hydrogen-terminated surface. This termination results in a 'negative electron affinity' (NEA), *i.e.* the conduction band minimum of the diamond is higher in energy than the vacuum level (Figure 7). This occurs due to electronegativity differences between carbon and hydrogen which results in the formation of a dipole layer at the surface of the diamond⁵²⁻⁵⁵ (Figure 8). By heating the diamond, electrons can be excited into the conduction band from which there is essentially no energy barrier into the vacuum level. The work function of hydrogen-terminated diamond is ~ 2 eV lower than a clean, carbon-only diamond surface (3 eV compared to 5 eV)^{52,53}. The low work function of hydrogen-terminated diamond leads to the diamond being an excellent thermionic emitter. Thermionic emission occurs when enough thermal energy is given to a charge carrier to overcome the work function of the material it is in. Diamond with a NEA could be utilised as a material for an emitter in a TEC as the NEA leads to ballistic electron emission, *i.e.* electron emission without a barrier, as once an electron has sufficient thermal energy there are no energy barriers for it leaving the material. This will give large electron yields which are necessary for an efficient TEC. Additionally, hydrogen-terminated diamond has been shown to have applications as a photo-catalyst for reduction of nitrogen⁵⁶ as well as producing high current, high brightness electron beams as a diamond amplifier cathode¹⁹.

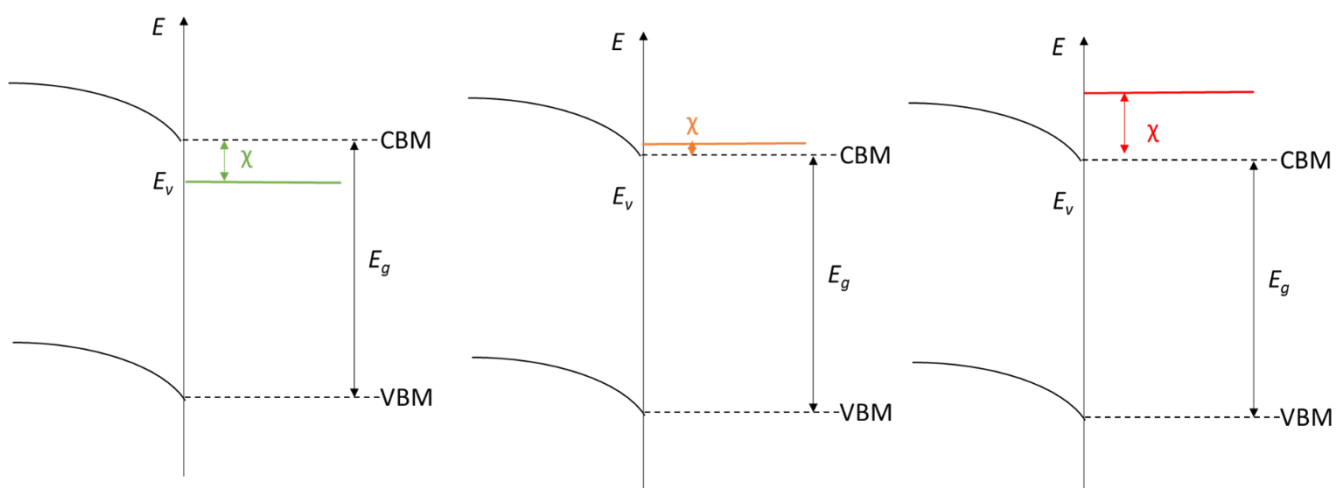


Figure 7: Schematic diagrams showing the difference between a negative electron affinity (NEA, left), an effective negative electron affinity (centre), and a positive electron affinity (right). E_v - vacuum level; χ - electron affinity; VBM - valence band maximum; CBM- conduction band minimum. Effective NEAs occur when χ is between 0 and 0.7 eV.

Despite its potential, there are some difficulties with using hydrogen-terminated diamond as a thermionic converter. Firstly, the work function of hydrogen-terminated diamond is too high for low

temperature electron emission. Any device using this material to produce electricity from solar or waste heat, which will be at relatively low temperatures, will have limited efficiency as the current generated is dependent on the electron emission.

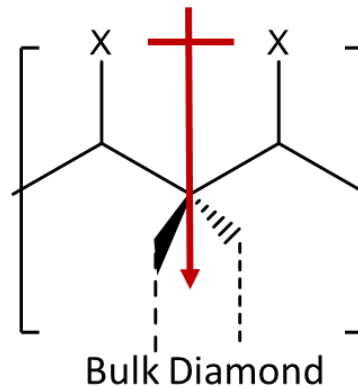


Figure 8: A cartoon demonstration the nature of the surface dipole necessary for formation of a NEA.

Secondly, the electron yield degrades slowly when the diamond is left in ambient atmosphere. This is due to oxygen from the air slowly replacing the hydrogen termination, reversing the surface dipole and giving a positive electron affinity. This happens even faster when the oxygen is excited in some way, *e.g.* UV light or thermal excitation⁵⁷⁻⁶¹. Additionally, hydrogen-terminated diamond can suffer from p-type surface doping (the transfer of an electron from an adsorbate to the material) when in air which can introduce a barrier to electron emission by upwards band bending⁶². Whilst thermionic converters are high vacuum devices, this instability in ambient atmospheres could cause issues with device fabrication as well as reducing the useable lifetime of the thermionic converter.

As a result, a variety of different metals and compounds have been used to terminate the diamond surface in an attempt to maintain the NEA and decrease the work function whilst introducing a stronger, more thermally stable bond. These include transition metals and their oxides⁶³⁻⁶⁷, alkali earth and alkali metals, alkali-halides^{68,69}, and alkali-oxides^{26,57,62,70,71}.

1.2.3.1 Transition Metal Terminations

One of the first transition metal adsorbates investigated was nickel, initially on non-conducting type IIa diamonds using ultraviolet photo electron spectroscopy (UPS) and low energy electron diffraction (LEED) methods which both rely on electron emission⁷². However, the samples did not yield an emission signal, which was thought to be due to charging issues that arise when using these techniques to analyse non-conducting surfaces. Consequently, conducting (111) and (100) orientation natural type IIb diamonds were used which were successfully characterised with no charging effects. These diamonds were first cleaned to remove physically adsorbed contaminants, such as metals, waxes, and gases. This was achieved by boiling in sulfuric acid and a saturated CrO₃ solution in sulfuric

acid, before etching in boiling *aqua regia* and subsequently annealing under vacuum. The temperature of this anneal was 850°C for the (111) diamond whilst the (100) diamonds were annealed at temperatures ranging from 545 to 1070°C. In an attempt to remove chemically adsorbed hydrogen on the (111) diamond, they were heated to 350°C and exposed to an argon plasma without removing them from vacuum. This was deemed to be successful give a clean, carbon only surface by the absence of a NEA peak when ultraviolet photoelectron spectroscopy (UPS) was performed. After cleaning, the nickel was deposited in the same vacuum system by thermal evaporation to thicknesses up to 2.5 Å onto the annealed (100) surfaces as well as onto the carbon only (111) surface and a hydrogen-terminated (111) surface. The exact method of this hydrogen exposure is unclear. During the deposition, the diamond itself was not heated to encourage complete coverage and prevent island formation.

On the hydrogen-free, nickel-coated (111) diamond surface, a NEA was observed at a maximum for a 1 Å thick layer whilst on a hydrogen-terminated nickel-coated surface, no NEA was observed. On the (100) surface, diamonds which were annealed above 900°C with a 1 Å thick layer of nickel showed the largest NEA. This temperature was shown to be the lowest temperature at which oxygen was desorbed.

The proposed explanation for the observations on the (111) and (100) diamonds was that chemically adsorbed hydrogen and oxygen species increased the Schottky barrier (*i.e.* the potential energy barrier at the diamond-metal surface) which effectively increases the energy of the vacuum level to above the CBM, removing the NEA.

In a similar experiment, Baumann and Nemanich investigated the effect of cobalt and copper deposition onto (100), (111), and (110) orientated natural IIb diamond^{59,64,67}. To clean the diamonds, they underwent an electrochemical etch followed by exposure to UV/ozone and rinsed in HF solution in a process analogous to the acid washing performed during the nickel experiments. Three different UHV methods were used to further remove adsorbed contaminants: 1) A 500°C anneal (performed only for the (100) orientation) which was assumed to leave an oxygen termination, 2) a 1150°C anneal shown to leave an adsorbate free, clean diamond surface, and 3) exposure to a hydrogen plasma which was also used to hydrogen terminate the samples. Cobalt and copper were deposited by electron beam and hot filament evaporation at room temperature to give films between 1 and 10 Å thick. UPS was used to determine whether the samples had a NEA and, in order to test stability, the samples were exposed to atmospheric conditions and re-analysed.

For cobalt, a maximum NEA was achieved using 2 Å of cobalt on a carbon only (100) diamond surface although all orientations and terminations led to a NEA. The only exception to this was the oxygen-

terminated sample which showed a positive electron affinity. As suggested previously, it could be that oxygen and hydrogen atoms are disrupting the interaction between cobalt and the diamond surface and increasing the Schottky barrier. Very similar results were obtained for the copper although a slightly larger maximum NEA was observed for 1 Å on the clean (110) surface. All samples saw a decrease in NEA after exposure to atmosphere but this stabilised, indicating good atmospheric stabilisation.

In the same manner, zirconium coatings were investigated⁶⁷. These gave NEAs for all terminations and orientations which were maximised when 1 Å of zirconium was deposited. The NEAs were much larger than for the much less reactive cobalt and copper alternatives. This observation appears to reinforce the hypothesis that hydrogen and oxygen adsorbates increase the Schottky barrier as zirconium's greater reactivity would allow it to displace any hydrogen or oxygen terminations on the diamond surface. The zirconium-induced NEA was found to be fairly stable when exposed to atmospheric conditions, similar to the copper and cobalt induced NEAs.

More recently, theoretical work has been carried out using density functional theory to model copper, nickel, vanadium, and titanium coatings on (100) diamond surfaces⁶³. This was done at 1, 0.5, and 0.25 monolayer coverages although the exact definition of a monolayer used is ambiguous. In this work, it was suggested that these four metals can be divided into two categories, those that interact strongly with the carbon surface and form carbides, and those that have a much weaker interaction. Both titanium and vanadium were shown to form carbides and these both gave NEAs at a low coverage whilst copper and nickel (non-carbide-forming metals) needed a much larger coverage to produce a NEA. It seems likely that carbide-forming metals will give much more thermodynamically stable compounds as these will form a strong, covalent bond with the diamond surface. Experiments carried out on late transition metals, such as nickel, copper and cobalt, reinforce this conclusion as they all showed relatively small NEAs at low metal coverages whilst the earlier transition metal reported experimentally - zirconium - behaves in a manner more similar to that predicted for titanium and vanadium.

For transition metals, it appears that a maximum NEA is formed using thin coatings of metal, on a clean, carbon only, diamond surface. Other adsorbates and terminating atoms increase the Schottky barrier between the diamond and the metal, increasing the energy of the vacuum level relative to the CBM and increasing the electron affinity. Interestingly, the orientation of the diamond surface appears to play a role in the formation of the NEA which could be due to the different surface structures determining how the metal sits on and interacts with the diamond. One theory is that by including other adsorbates between the metal and diamond surface the distance between the metal

and diamond is increased. This will give a dipole with a smaller magnitude and so a decrease in electron affinity occurs. The same logic can be applied to the different diamond reconstructions and crystal planes as certain arrangements could allow the metal to sit closer to the surface. The theory that carbide-forming metals give a larger NEA at smaller coverages than their non-carbide forming counterparts complements the idea of metal-diamond distance having a large effect on electron affinity. Metals forming a covalent bond with the diamond would be closer to the surface than those which do not form a formal bond.

One area that seems to be lacking research is the possibility that the morphology of the diamond and deposited films could play a role in any electronic properties.

1.2.3.2 Group 1 and 2 Metal and Related Compound Terminations

Alkali halides

Wang *et al.*⁶⁸ studied the deposition of lithium fluoride onto HFCVD boron-doped polycrystalline diamond. The strength of the lithium-fluorine bond would allow for easy and clean deposition which would be useful in device fabrication and, so long as the lithium fluoride was present in the right orientation, the molecule's large dipole moment could induce a perpendicular surface dipole, resulting in a NEA. This work was carried out on both hydrogenated and oxygenated diamond samples which were annealed at 150°C in UHV to remove any adsorbed gaseous contaminants, before deposition by thermal evaporation of lithium fluoride, also in UHV. More rigorous cleaning procedures, such as those undertaken for single-crystal and natural diamonds, would be unnecessary for newly synthesised and unpolished polycrystalline diamond. Such samples would not have metal or wax contaminants which acid washes are used to remove.

The lithium fluoride deposition was carried out in stepwise fashion, with measurements of work function (using Kelvin Probe force microscopy) and ionisation potential (using UPS) taken between each increment using Auger electron spectroscopy to monitor the thickness of the layer. When present in only a few angstroms, the LiF greatly reduced the work function of the diamond and imparted a NEA (as shown by a low energy electron emission signal from below the energy of the CBM of diamond) on both oxygen- and hydrogen-terminated diamond samples. As the thickness of the layer increased, the work function of the material also decreased at a falling rate. This is due to additional lithium fluoride forming islands and clusters instead of interacting with the diamond surface. The measured work function reached a minimum which was equal to that of bulk lithium fluoride *i.e.* the work function being measured was that of lithium fluoride not the diamond-lithium fluoride surface.

Given the decrease in work function and the emergence of a NEA upon lithium fluoride deposition, it seems likely that that lithium fluoride is interacting in the correct orientation with the diamond to give a perpendicular surface dipole. It is also thought that lithium fluoride causes band bending in the diamond which contributes to the NEA and the decreased work function. However, no work was done looking into the thermal and atmospheric stability of these films and it seems likely that the lithium fluoride molecules will only be physisorbed to the diamond surface and will lack stability. Wang *et al.*⁶⁹ [ref] also studied films of rubidium fluoride, this time only on hydrogen-terminated diamond samples. This was done in an almost identical manner and it was found that a rubidium fluoride film significantly reduced the work function of diamond in a manner analogous to the early stages of lithium fluoride deposition. However, above a monolayer very little change was seen which could be due to a change of phase or orientation of the rubidium fluoride surface and a NEA was never achieved^{68,69}.

Alkali metals and oxides

Food *et al.*⁷³ looked into a barium coating on a type IIb single crystal natural diamond (111). The diamond was acid cleaned and annealed at 1000°C in UHV before being coated in barium using a barium getter. A variety of different coverages were deposited between 1.45 - <0.001 monolayers. A NEA was observed for all coverages below a monolayer but this was quenched when over a monolayer. When over half a monolayer was deposited, charge transfer from barium to diamond resulted in significant downwards band bending. If this was the only effect occurring, the CBM would be below the vacuum level and no NEA would be observed. In order to produce a NEA as observed, the surface dipole between barium and diamond must be large enough to counterbalance this downwards band bending and keep the CBM below the vacuum level.

The oxygen present from acid washing was shown not to be involved in formation of a reactive interface between barium and diamond as the oxygen core-level binding energies were shown to change very little throughout the process. The barium coating had a very good thermal stability, not fully evaporating even when annealed at 1150°C. This lack of interaction with oxygen adsorbates indicated that the barium binds as some kind of carbide, giving a strong bond between the diamond surface and barium atoms, although no work was carried out on whether the NEA was retained after heating⁷³.

Food *et al.* also carried out work looking at caesium on oxygen-terminated, predominately (111), undoped polycrystalline diamond and characterised them using ultraviolet and X-ray photoelectron spectroscopy (UPS and XPS)⁷⁰. Caesium was evaporated under UHV using a caesium getter to give a monolayer of caesium on three different diamond surfaces. One was acid cleaned in a boiling mixture

of nitric and sulfuric acids followed by a 1127°C anneal in vacuum, another was exposed to atomic oxygen at room temperature to achieve an oxygen termination, whilst the last was exposed to atomic hydrogen also at room temperature to give a hydrogen termination. It was assumed that the acid-cleaned surface would be a clean, carbon surface formed by rearrangement of the (111) surface to give carbon-carbon double bonds. Whilst it seems likely that the acid-cleaning step would result in oxygen terminations, given the oxidising power of such concentrated acids and subsequent procedures⁵¹, such a hot anneal is likely to remove most of this adsorbed oxygen. The stability of the caesium-coated surfaces were studied by exposing them to atmosphere followed by heating.

All three of these diamond surfaces exhibited a NEA, however, the diamond-hydrogen-caesium surface had a much smaller NEA than the diamond-oxygen-caesium and diamond-caesium terminated surfaces. Both the oxygen-terminated and acid-washed samples had a slight reduction in NEA upon exposure to atmosphere, thought to be due to the formation of insulating Cs-oxides, but the resulting lower NEA was fairly stable to further exposure. When heated, the NEA persisted up to 660 K for these two samples before being lost. In contrast, the hydrogen-terminated sample was much less stable, losing its NEA entirely upon exposure to atmosphere. When heated to 370 K the NEA was regenerated thanks to the evaporation of insulating oxides formed upon exposure to air but lost again upon further heating to 470 K.

These results were mirrored by Geis *et al.*⁷⁴ who looked at caesium coatings on a variety of different diamond samples in terms of their field emission. These include lithium-doped (100) and boron-doped (100) and (111) homoepitaxial HFCVD diamond as well as nitrogen-doped type IIb high pressure synthetic diamond. These samples were all cleaned in boiling sulfuric and hydrogen peroxide before being exposed to oxygen or hydrogen plasma in vacuum to terminate the surface. These samples were then annealed at 200°C and caesium was deposited using a caesium getter until the field emission of electrons from the diamond stopped changing. The caesium-coated diamonds were next heated to >200°C and exposed to an oxygen atmosphere in order to test their stability. The electron-emission results echo findings of Foord *et al.* with a larger, more stable current measured for the oxygen-caesium-terminated diamonds than the clean diamond surface.

The larger and more stable electron emission when using an oxygen-terminated sample can be explained by how the caesium interacts with the diamond surface. On an oxygen-terminated surface a stable C-O-Cs salt with a large dipole that reduces the work function can form. Caesium on a hydrogen-saturated surface will lower the work function just by sitting above the surface and creating a smaller dipole but will not form any kind of bond. This means it will be easily evaporated when heated causing the work function to increase.

Further work has also been carried out looking at the adsorption of potassium onto both a clean diamond surface⁷⁵ and hydrogen- and oxygen-terminated surfaces⁵¹. A clean diamond surface was prepared by growing a film of boron-doped MWCVD on top of a natural single-crystal type IIb diamond. Such films are usually hydrogen terminated and so a 1400 K anneal in UHV was used to desorb hydrogen. Potassium was deposited by thermal evaporation to give between 0.05 and one monolayer of potassium (where a monolayer is defined as 5.60×10^{14} atoms cm^{-2}) on the diamond surface. Work function was measured using thermal desorption spectroscopy and, from these measurements, the electron affinity was calculated. A maximum NEA was calculated when half a monolayer was deposited and this NEA began to decrease above that.

The hydrogen- and oxygen-terminated diamond surfaces were prepared on a type IIb (100) natural diamond by exposure to hydrogen plasma and acid washing, respectively. Potassium was thermally evaporated in UHV although the thickness or extent of coverage of the film is unclear from the literature. A NEA was observed for the hydrogen-terminated sample although this was smaller than for the potassium-free, hydrogen-terminated diamond sample. In the case of oxygen, a positive electron affinity was detected. Changes in the energy of the O 1s peaks in the XPS spectrum appear to indicate the formation of a salt-like structure containing $\text{K}^{\delta+}$ which is in agreement with earlier postulations on the nature of the Cs-O-diamond interaction.

Theoretical work by O'Donnell *et al.*²⁶ predicted that a lithium-oxygen monolayer (one lithium atom per oxygen atom) on a (100) surface would give a substantial NEA with a much higher binding energy than those seen for caesium-oxygen layers. This work was carried out using DFT calculations on intrinsic diamond and modelled both ketone and ether-bridging oxygen terminations. It appears as though lithium is accommodated with minimal structural distortion which is different to heavier alkali-metal interactions. Materials such as caesium cause substantial structural distortion due to their size which results in different electronic effects. Using projected density of states, the lithium bonding was predicted to be ionic involving Li^+ which would give a large binding energy between lithium and the oxygen-terminated diamond sample. As a result, such a film was predicted to be very stable. In such a scenario, the lithium would be fully oxidised which would further increase the film's stability as the likelihood of fully oxidised lithium being attacked by adsorbates is low.

This work was verified experimentally by O'Donnell *et al.*^{50,57} using type IIa (100) single-crystal diamond with a boron-doped layer of diamond grown epitaxially above it. This was acid cleaned before being oxygen terminated by either exposure to oxygen plasma, ozone, or acid washing. All of these different methods were shown to give slightly different kinds of oxygen terminations but with a high oxygen coverage. From here, two different methods were employed to deposit lithium films. The first

of these, coined the 'thick film method', involved deposition of lithium by thermal evaporation under a moderate vacuum to give a film between 50 and 200 nm thick. Under such conditions the film reacted to form a surface layer of lithium oxides which were used to protect the lithium-diamond interface when later exposing the sample to air. Excess lithium was dissolved off using high purity deionised water to leave a monolayer coverage which was then transferred to UHV for XPS and UPS measurements. XPS showed that the residual lithium was different to the as-deposited lithium indicating surface chemistry is occurring between lithium and the diamond surface, supporting the predictions made during the theoretical work of an ionic interaction. Evidence from UPS measurements suggested a large NEA, equivalent to a hydrogen-terminated diamond surface. However, using this method there were problems with reproducibly producing a diamond film with a NEA.

In order to address these issues the 'thin film method' was developed. Oxygen-terminated diamond was transferred to UHV and annealed at 300°C to remove weakly adsorbed contaminants before lithium was deposited using a getter to give sub-monolayer coverages. This lithium-coated sample was then analysed by XPS and UPS and, intriguingly, little difference in electron yield and work-function between the non-lithium-coated diamonds was observed. In order to facilitate any change in electron affinity and work function the surface needed to be activated by annealing it. A maximum NEA was induced by annealing the surface at 800°C which was confirmed by total photoelectron yield spectroscopy. The coated sample was next exposed to air and re-analysed. Only a slight decrease in NEA was observed which was quickly reversed by a moderate, 300°C anneal. However, it is postulated that the lithium surface would suffer from long-term hydroxylation if removed from UHV indefinitely and the need to anneal such a surface would make it difficult to regenerate the surface *in situ* after it has been in use for some time.

In later theoretical work, further alkali earths and alkali metals were investigated in the same manner as the theoretical work on lithium-oxygen terminations. Sodium, potassium, caesium, and magnesium coatings were all modelled on oxygen-terminated diamond surfaces, assuming all oxygen terminations would be the more favourable ether bridge⁷⁶. The first point of note is that the maximum coverage possible varies depending on the size of the adsorbate. Only lithium and sodium were able to form a monolayer (*i.e.* had a negative energy of adsorption at coverages for one metal atom per oxygen atom), and even sodium was not so well incorporated into the surface structure and had a stronger adsorption energy at 0.5 monolayer coverage. Whilst a half monolayer was found to be most favourable for magnesium, there were a lot of similarities between it and a lithium monolayer in terms of incorporation within the surface structure. This is not so surprising considering they are both smaller atoms and have very similar solid-state chemistries. Whilst the heavier atoms exhibited a

structure indicative of carbon-oxygen double bonds without a dimer surface reconstruction, the lighter atoms gave a structure containing carbon-oxygen single bonds with a dimer surface reconstruction. Evidently, neither of these scenarios involves the ether bridge oxygen termination which seems likely to be the most stable geometry. This could explain the need to anneal lithium-coated substrates in order to generate a NEA, as the energy could be needed to overcome the barrier between ether bridge structures and the more stable and polar carbon-oxygen-lithium structure.

In principle, one would expect the more electropositive, heavier atoms to induce a larger dipole and so decrease the work-function the most. However, what was found was that the lighter lithium and magnesium atoms gave a larger NEA, indicative of a larger surface dipole. In order to understand this slightly counter-intuitive idea, the authors explored the different geometries of the adsorbates and how this affected their electronic structures.

Firstly, it is necessary to understand the nature of the dipole between the carbon, oxygen and adsorbate. In all cases, the positive part of the dipole is centred over the oxygen-metal bond whilst the negative is centred over the carbon-oxygen bond. However, in the case of the heavier metals there is a second dipole between the ions and other oxygen-metal bonds. The negative part of this second dipole partially cancels the positive part of the first which gives some explanation for why the lighter metals give a larger dipole. Further to this, the lighter metals are better incorporated into the surface structure (Figure 9) which lowers the energy of the oxygen lone pairs. This allows the lone pairs to overlap with the diamond valence band which enhances the negative charge on the carbon-oxygen bond. This increases the charge separation perpendicular to the surface resulting in a larger dipole. Caesium and potassium are classified as heavier metals whilst magnesium and lithium are lighter. Sodium acts as an intermediate in this case, being reasonably well accommodated within the surface structure.

Building on this work, O'Donnell et al investigated the effects of a magnesium film. This was carried out experimentally in exactly the same way as the thin film method used for lithium deposition using both oxygen plasma and acid washing to oxygen terminate the surface. A maximum NEA was found for a half monolayer coverage on an oxygen -terminated surface. In fact, this is the largest ever reported NEA for a diamond surface of -2.0 eV. Greater coverages had a lower NEA caused by surface depolarisation due to the Mg-O-C dipoles interacting with one another, as mentioned above for caesium and potassium coverages. Interestingly, no anneal was needed to activate the surface and a NEA was observed as soon as magnesium was deposited; even when it was annealed there was no evidence for the well-ordered domains formed by lithium. This is due in part to the different way the bonds are formed. Magnesium forms much stronger bonds and so it may not be possible to re-organise them without desorption of magnesium. This explains the absence of well-ordered domains; even when the magnesium is annealed it covers the diamond surface in a random manner. The fact that magnesium bonds are stronger could play a part in why no activation is necessary to obtain a NEA. However, given the previous explanation for why this activation is needed for lithium, one would expect that an energy barrier would have to be overcome to give the correct carbon-oxygen-magnesium bonding for the necessary dipole for a NEA.

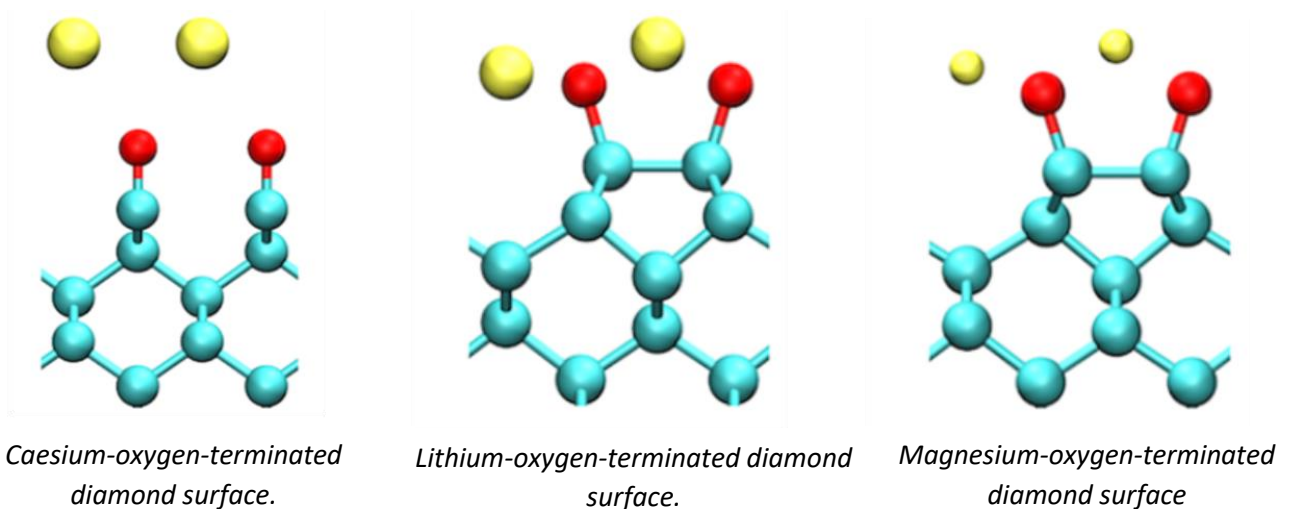


Figure 9: An adapted figure from O'Donnell et al to illustrate the difference between the structures of different metal-oxygen diamond terminations ⁷⁶.

After exposure to air the NEA is slightly diminished although it is still large and is almost fully regenerated when annealed in UHV. The small decrease is partly because the coverage is enough to prevent surface-transfer doping from adsorbed molecules and upwards band bending. When immersed in water the NEA is hugely decreased, due to the depolarising effect of adsorbed water molecules, but the electron yield is minimally effected as the NEA is retained

Whilst the oxygen plasma and magnesium deposition gave the largest NEA, the acid-washed sample still gave a respectable NEA. The lower NEA is in part due to greater upwards band bending which has been assigned to hydroxyl groups, not present when using oxygen plasma, initially preventing magnesium adsorption.

The use of magnesium to induce a NEA is very exciting as so little Mg is required and a NEA is induced without an annealing step. The lack of annealing step means that that it could be very easy to regenerate the surface *in situ* even in hostile environments. The work described above indicates that light metals deposited onto oxygen terminated diamond surfaces in monolayer to sub-monolayer quantities have been the most successful in inducing a large and stable NEA. Aluminium terminations have never been studied and this metal would appear a good candidate for inducing a NEA on diamond.

1.3 Theoretical Concepts

In order to model the electronic structure of a material it is necessary to solve the full electronic Hamiltonian,

$$H = \sum_i \left(-\frac{1}{2} \Delta_i - \sum_{\alpha}^K \frac{Z_{\alpha}}{|\vec{r}_i - \vec{R}_{\alpha}|} \right) + \frac{1}{2} \sum_{i \neq j} \frac{1}{|\vec{r}_i - \vec{r}_j|}. \quad (3)$$

The first two terms describe the kinetic energy and the electron-nucleus interactions. As both these are one-particle terms they can be solved exactly using mean-field theory. Mean-field theory is a method to reduce many-body problems to one-body problems and does this by reducing a system to a large number of individual components which interact with one another. The effect of all other individuals on a given individual can be approximated as a single, average effect. The final term gives the electron-electron interactions and this can only be solved approximately using the mean-field theory as this is a real many-body term.

Density functional theory (DFT) solves the full electronic Hamiltonian using functionals of electronic density. This is possible as the ground state energy of a system can be expressed as a functional of the ground-state electron density of the system and this, in principle, makes DFT an exact method. However, DFT begins to break down when the electron density is not homogenous, as is the case in insulators and semiconductors. There are a number of approximations and functionals which allow DFT to give better solutions of the electronic Hamiltonian for these materials. However, the exact exchange and correlation functionals (required for the electron-electron interaction term in the Hamiltonian) are not known and consequently empirical terms are added to improve their accuracy. These all suffer from the same limitation, that the correlational functional is not systematically improvable. Consequently, an informed trial-and-error process is used to improve the accuracy of DFT

which, by its very nature, is not systematic. Another issue with DFT is that it is intrinsically poor at predicting electronic structure based on excited states, such as band gaps. This arises from its being a ground-state theory (it is based on the fact the ground-state energy is a functional of the ground-state electron density) which inaccurately models excited states.

In contrast wavefunction methods are systematically improvable as the nature of the exchange correlation term is known. These methods work using mean-field theory to model the interaction of an individual electron on all other electrons, unlike DFT which uses electron density. Wavefunction methods predict the correlation between electrons much more accurately than DFT because they are based on the correlation between individual electrons rather than regions of electron density. The accuracy of such methods is further improved by increasing the size of the field of influence of an electron and this is the basis of methods such as MP2 theory and coupled-cluster theory. Wavefunction theory is also able to calculate energies of excited states much more accurately than DFT as it does not rely on the principle that the ground-state energy is a functional of the ground-state electron density. However, wavefunction methods are much more computationally expensive and the cost scales with between N^5 and N^8 (depending on the method used) where N is the number of electrons. To put that into perspective, in a diamond lattice if only the fourth-nearest neighbours were considered, that would be 64 atoms each with 4 interacting electrons giving a total of 256 electrons. A variety of different methods have been developed to try to utilise wavefunction theory for bulk materials whilst reducing the computational cost. One such method is the hierarchical method^{77,78}.

1.3.1 The Hierarchical Method

The hierarchical method is a way of extending molecular electronic structure methods to the solid state. It was first applied to orthorhombic blocks of lithium hydride (LiH) with dimensions $l \times m \times n$ to calculate the cohesive energy of the infinite crystal. It works by breaking the cohesive energy (E^{tot}) into two parts, the Hartree-Fock contribution (E^{HF}) and the correlation contribution (E^{corr}),

$$E^{tot} = E^{HF} + E^{corr}. \quad (4)$$

The Hartree-Fock energy can be calculated using standard methods but the correlation energy needs to be decomposed further into the sum of the correlation energy of each LiH molecule (E_{mol}^{corr}) and a term described as the 'correlation residual' (ΔE^{corr}),

$$E^{corr} = \frac{1}{2}lmnE_{mol}^{corr} + \Delta E^{corr}. \quad (5)$$

The correlation of the LiH molecule can be computed accurately whilst the correlation residual is defined as:

$$\Delta E^{corr} = c^{000} + c^{001}(l + m + n) + c^{011}(lm + ln + mn) + c^{111}lmn. \quad (6)$$

From this it can be seen that the contribution of correlation residual per ion pair is $2c^{111}$. By calculating the energies of different sized cluster (*i.e.* different values of lmn) it is possible to produce a set of simultaneous equations which can be solved to find each of the correlation coefficients. Once c^{111} is found, the correlation residual can be calculated and it is then a simple matter to solve equation (4) to find the total cohesive energy.

This procedure was carried out for LiH by building unique orthorhombic clusters with dimensions lmn and using MP2/ cc-pVTZ to calculate the energies. For a given number N , the clusters were ordered lexicographically, where $lmn \leq N$, and the last 4 clusters were selected to solve the simultaneous equations. This was done because it would provide the most bulk-like clusters which would converge upon the bulk value fastest. Clusters were grown in a systematic way keeping l and m constant whilst increasing n . The result for the calculated cohesive energy per formula, -0.176 a.u., was in good agreement with experimental value of -0.175 a.u. It is also indicated that some success has been had in carrying out similar calculations with lithium fluoride and magnesium oxide^{79,80}.

The hierarchical method has also been applied to calculating the cohesive energy of crystalline neon⁸¹, which adopts a non-ionic face-centred cubic crystal. It was found that the bulk cohesive energy converged once again, indicating that the method is valid for such a system. However, in order to reduce the errors in the calculated cohesive energies, larger clusters were required and higher-order terms were important in accurately predicting the bulk energy. These two factors are slightly problematic as they increase the computational cost of applying the hierarchical method.

1.4 Project Objectives

The following investigation is an attempt to prepare a low work function, thermally stable material from diamond using an adsorbed aluminium-oxygen layer to induce a negative electron affinity. Another aspect of the project is to test the application of the hierarchical method to diamond to calculate the band gap of diamond.

2 Experimental Materials and Methods

2.1 Materials

The 1-3 micron diamond powder used during this investigation was from Diadust, Van Moppes, Geneva. The p-type silicon wafer used was from Si Mat. It was boron doped, polished on a single side with a thickness of $500 \pm 25 \mu\text{m}$ and a resistivity of 1-10 $\Omega \text{ cm}$. The molybdenum foil used was annealed and had a thickness of 0.5 mm from Goodfellow Cambridge Ltd., Huntingdon, England. The tantalum wire was from Advent Research Materials Ltd., Oxford, England and had a purity of 99.9% and a 0.25 mm diameter. The nanodiamonds used were purchased from Microdiamant AG whilst the carboxyethylsilanetriol was purchased from Fluorochem Ltd. Both methane (CP grade) and nitrogen (Research grade) gas had a purity of 99.99% and were purchased from BOC. The hydrogen gas used came from Air Liquide and was CP grade with a 99.995% purity.

2.2 Chemical Vapour Deposition (CVD)

2.2.1 Substrate preparation

Substrates were seeded for diamond growth in two ways.

Method 1: This was carried out using only silicon substrates which were abraded by rubbing two pieces of silicon over one another with 1-3 micron diamond powder in between⁸². Once completed CVD was carried out immediately.

Method 2: The substrate was seeded with a nanodiamond suspension. The substrates were first cleaned by submerging them in acetone and sonicating them for 5 min using an ultrasonic bath before rinsing in double-deionised water (in both cases using glass beakers) and drying using a compressed air gun. Substrates were then placed in 20% (v/v) solution of carboxyethylsilanetriol (disodium salt) in water (in a plastic container) with the desired growth side face up for 15 min. Once this was completed, the substrates were rinsed in deionised water before being deposited in a nanodiamond sol (0.018 μm diamond in water, 25 cts kg^{-1} , in a plastic container) for 5 min with the growth side face up. Following this, substrates were rinsed in deionised water and dried⁸²⁻⁸⁴. Once seeded, these substrates were stored in plastic boxes under ambient conditions before CVD.

2.2.2 Undoped Hot-filament CVD

Undoped polycrystalline diamond was grown on seeded p-type (100) silicon wafers. This was achieved using a hot filament reactor (Figure 10) with tantalum filaments which was first evacuated to roughly 7.5×10^{-2} torr (1 torr = 133.332 Pa) with the silicon substrates 4 mm below the filaments. Once this pressure was reached, hydrogen and methane were allowed into the reactor at 1% (v/v) methane in hydrogen and the pressure of the reactor was maintained at 20 torr. Once the gases were introduced

to the chamber, a current of 25 A was put through the tantalum filaments which resulted in a voltage of between 11 and 6 V. The growth time was seven hours and the samples were left to cool for around 30 min in a hydrogen only atmosphere. Once the growth time was complete, optical microscopy was used to ensure that diamond had been successfully produced. The samples were stored in plastic boxes under ambient conditions^{82,83}.

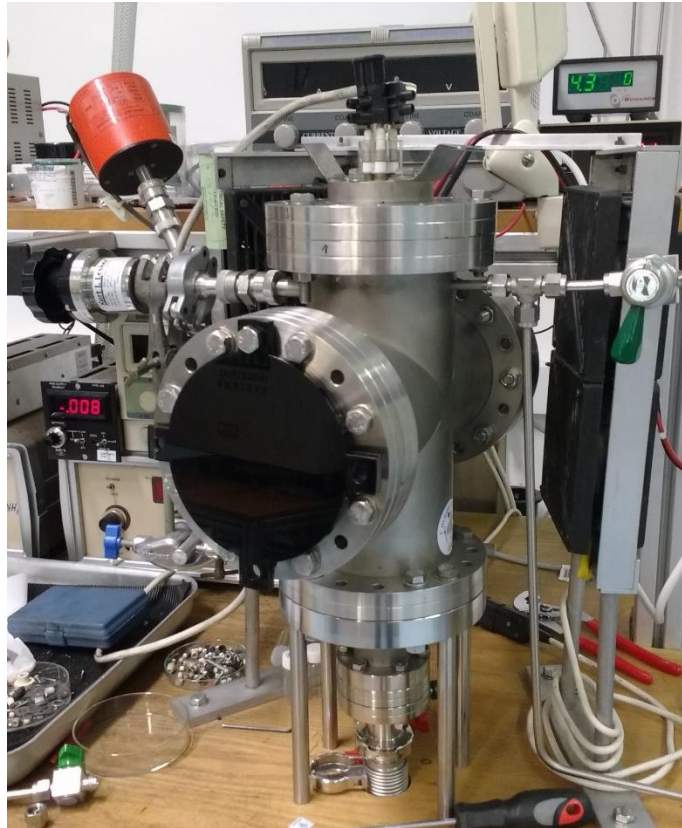


Figure 10: Hot filament CVD reactor.

2.2.3 Nitrogen-doped Microwave Plasma CVD

Nitrogen-doped polycrystalline diamond was grown by CVD on nanodiamond-seeded molybdenum substrates in a microwave reactor (Figure 11). This was carried out by first evacuating the chamber of the microwave CVD reactor to a pressure of less than 10×10^{-2} torr, before hydrogen, methane, and nitrogen were introduced at 4.2% (v/v) methane in hydrogen and a 2.5% (v/v) nitrogen in hydrogen. The growth was carried out at a microwave power of 1300 W and a pressure of 130 torr for 15 min. The molybdenum substrates were estimated to reach around 850°C and were left in a hydrogen atmosphere to cool^{82,83}. Following growth, the samples were stored in plastic boxes under ambient conditions.

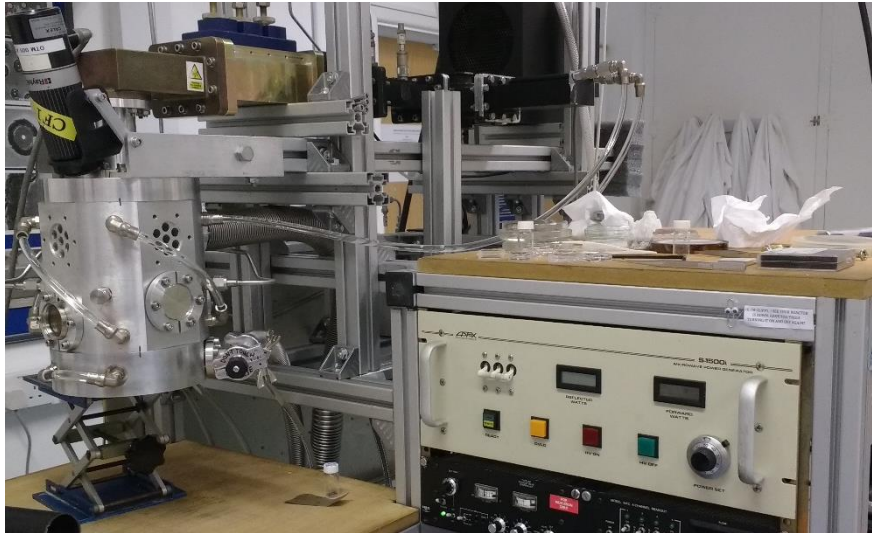


Figure 11: Microwave plasma CVD reactor.

2.4 Raman spectroscopy

Raman spectroscopy utilises a laser which interacts with the sample. Information is gained about the sample by the change in energy of inelastically scattered photons due to an energy transition within the sample. Raman differs from conventional spectroscopic techniques in that photons are not absorbed and emitted and the radiation measured is not in resonance with the energy transitions of the material. This results in quite different information being collected as the effect is not dominated by one transition moment, instead being influenced by a variety of different transitions from rotational to vibrational and even electronic transitions, although the main transitions are the vibrational⁸⁵. Raman can be used to characterise the type of bonding present in a material, allowing sp^3 hybridised carbon from diamond to be distinguished from sp^2 hybridised carbon from graphite.

Raman spectroscopy was carried out using a 514 nm green laser on a Renishaw 2000 spectrometer and data analysed using the Wire 2.0 package.

2.5 Scanning electron microscopy (SEM)

SEM can be used to obtain images of greater magnification and resolution than is possible with optical microscopy due to the smaller wavelength of electrons compared to visible light. Scanning electron microscopes work by illuminating the sample with a beam of electrons which are focussed using electron optics (magnetic and electric fields). These electrons interact with the sample, being scattered by it, analogous to an optical microscope, and causing emission of secondary electrons and electromagnetic radiation. The secondary electrons are detected and give topographical and morphological information on the sample whilst the backscattered electrons give information on compositional differences. In the case of polycrystalline samples, these backscattered electrons result in the contrast seen for different crystal planes. SEM is a high-vacuum technique and works best with

a conducting sample. It can be used in the case of diamond thin films to give an estimate of the thickness of such films as well as characterising the size and quality of the diamond crystals.

SEM images were taken using the JEOL JSM-IT300 instrument and with the Zeiss Sigma HD VP Field Emission SEM.

2.6 Energy-dispersive X-ray Spectroscopy (EDX)

This technique gains information about a sample by stimulating the emission of X-rays from the atoms in the sample using an incident high-energy beam of electrons. These electrons cause the ejection of an electron resulting in an electron hole. When an electron from a higher energy state relaxes to fill this hole, the difference in energy between the higher energy state and the hole is emitted as an X-ray. The difference between the energies of these states and, therefore, the energy of the emitted X-rays is characteristic for each element. By measuring the energy of the emitted X-rays, information can be gained on the elemental composition of the sample.

EDX was carried out in the JEOL JSM-IT300 SEM under the same conditions as stated above.

2.3 Surface derivatisation

2.3.1 Oxygen Termination

Oxygen terminations of diamond samples were carried out in a converted Edwards sputter-coater (Figure 12). Samples were first cleaned by sonication in ethanol, acetone and deionised water as described above, before being placed within the sputter-coater. The chamber was then evacuated to around 10^{-2} torr. Oxygen was then allowed into the chamber at a flow rate of 10 sccm and an oxygen plasma was struck using an electric current. The diamond samples were exposed to the oxygen plasma for between 5 and 7 seconds. Following oxygen termination, the samples were stored in plastic boxes under ambient conditions ⁴⁸.



Figure 12: Converted Edwards sputter coater used for oxygen termination.

2.3.2 Hydrogen Termination

Hydrogen terminations were carried out in the microwave CVD reactor on the nitrogen-doped polycrystalline diamond samples. First, the reactor was evacuated to a pressure of $15\text{-}20 \times 10^{-3}$ torr. This was followed by the introduction of hydrogen at 100 torr pressure. A plasma was struck using microwaves with a power of 1251 W. These conditions were maintained for two mins before the hydrogen pressure was reduced to 30 torr and the power reduced to 700 W. These conditions were maintained for a further two mins before the power was reduced to 0 W for a further two mins. Samples were then left to cool for a few mins before being removed from the reactor and stored in plastic boxes under ambient conditions^{82,83}.

2.3.3 Aluminium Deposition and Etching

Aluminium deposition was carried out using an Edwards bell jar evaporator (Figure 13). Diamond samples were placed roughly 10 cm away from a tungsten filament coated in aluminium with a direct line of sight to the filament. The bell jar was then evacuated to a pressure of around 10^{-6} torr before a 20 A current was passed through the filament to cause it to glow. Layers between 15 and 100 nm were deposited and the thickness of these layers was monitored *in situ* using an Agar quartz crystal resonator. Once the desired thickness of aluminium had been deposited the current was switched off and the whole apparatus left to cool down.



Figure 13: Edwards bell jar evaporator used for aluminium evaporation.

Once cooling was complete the aluminium coating was etched away by sonicating the sample in 1.2 M hydrochloric for between 10 min and 3 h. After etching, the samples were stored in plastic boxes under ambient conditions.

2.6 X-ray Photoelectron Spectroscopy

XPS (Figure 14) is an ultra-high vacuum process and uses monochromatic X-rays incident on the surface to cause photoelectron emission of both valence and core electrons of surface atoms. The core electrons are not hugely affected by their surroundings and their binding energies are characteristic of the elements they come from. By measuring the kinetic energy of these electrons, it is therefore possible to determine the composition of the surface. The environment does have a slight effect on their binding energy and separate peaks for the same elements bonded in different ways are observed. However the chemical shift is not always large enough to resolve the different signals into separate peaks⁸⁶.

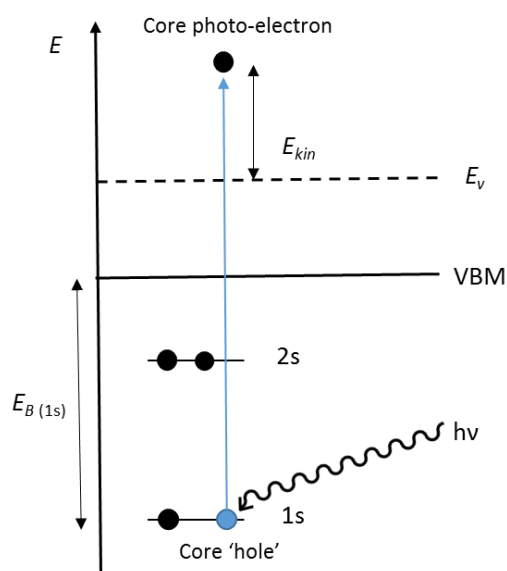


Figure 14: X-ray excitation of a 1s core electron. E_B is the binding energy, E_{kin} is the kinetic energy, E_v is the energy of the vacuum level and VBM is the valence band maximum.

X-ray photoelectron spectroscopy measurements were made using the nanoESCA II instrument (Scienta Omicron GmbH). Pressures were in the order of 10^{-9} and 10^{-10} torr and samples were annealed at 300°C prior to analysis. Measurements were made with X-rays from an aluminium $K\alpha$ source which gave photons with an energy of 1486.7 eV at an angle of 85° to the sample. The angle between the analyser and the sample was 20° . The sampling depth of the XPS varies depending on the material and angle between analyser and sample. In this case, the measurements sampled ~ 9 nm into the sample.

2.7 Thermionic Emission Measurements

Thermionic emission measurements were made using a thermionic energy converter, as described in section 1.1, on nitrogen-doped diamond films grown on a molybdenum substrate. The backside of the molybdenum substrate was patterned with a $10.6 \mu\text{m}$ grating using a laser cutter (Oxford Lasers, A series) in order to efficiently absorb the light from the laser heater. Following this, the diamond surfaces were re-terminated with either hydrogen, oxygen, or aluminium-oxygen terminations. The

thermionic emission testing was carried out at between 2.5×10^{-7} torr and 3×10^{-6} torr and the samples were heated using a 10.6 μm carbon dioxide laser. The temperature of the sample was monitored using an optical pyrometer and ramped from 300-600°C before dropping back down to 300°C and repeating 20 times. The working distance between the sample and the steel collector was 200 μm and a 25 V bias was applied to overcome the space-charge effect⁸³.

3 Results and Discussion

To achieve the project objectives (see 1.4) several polycrystalline diamond thin films were produced by CVD using either silicon (DFSi 1-5) or molybdenum (DFMo 1-3) as a substrate (1) and characterised to ensure their purity. These substrates were chosen because their thermal expansion properties are sufficiently like diamond to prevent delamination of the diamond film upon cooling or heating.

Sample	Substrate Type	Diamond Type	Surface Treatment	Etching Conditions 3
DFSi 1	Silicon.	Hot filament, undoped, microcrystalline.	Oxygen plasma termination followed by ~ 12 nm aluminium deposition.	1.2 M HCl with sonication for 3 hours.
DFSi 2	Silicon.	Hot filament, undoped, microcrystalline.	Oxygen plasma termination followed by ~ 12 nm aluminium deposition.	1.2 M HCl with sonication for 1 hour.
DFSi 3	Silicon.	Hot filament, undoped, microcrystalline.	Oxygen plasma termination followed by ~ 12 nm aluminium deposition.	No etch.
DFSi 4	Silicon	Hot filament, undoped, microcrystalline.	Oxygen plasma termination followed by ~ 100 nm aluminium deposition.	1.2 M HCl with sonication for 3 hours.
DFSi 5	Silicon	Hot filament, undoped, microcrystalline.	Oxygen plasma termination followed by ~ 100 nm aluminium deposition.	1.2 M HCl with sonication for 1 hour.
DFMo 1	Molybdenum	Microwave plasma, nitrogen doped, nanocrystalline.	Oxygen plasma termination.	No etch.
DFMo 2	Molybdenum	Microwave plasma, nitrogen doped, nanocrystalline.	1) Hydrogen plasma termination. 2) Oxygen plasma termination followed by ~ 100 nm aluminium deposition.	1) No etch. 2) 1.2 M HCl with sonication for 10 minutes.
DFMo 3	Molybdenum	Microwave plasma, nitrogen doped, nanocrystalline.	Oxygen plasma termination followed by ~ 100 nm aluminium deposition.	1.2 M HCl with sonication for 1 hour.

Table 1: Details of the different diamond thin films produced and the conditions used to alter their surfaces. The etching conditions are those used after surface treatment.

The DFSi diamonds were grown by hot filament CVD and then used to develop a method of aluminium-oxygen termination. In addition, nitrogen-doped diamond films were grown on a molybdenum substrate (DFMo 1-3) using microwave plasma CVD to compare the thermionic emission properties of diamond with the aluminium-oxygen termination to hydrogen and oxygen terminations.

Molybdenum was used because its high melting point allowed electron emission to be tested at temperatures above the melting point of silicon. Since nitrogen doping raises the Fermi level, which aids in thermionic emission, it was used to increase the thermionic current measured and reduce the error in these data. It had been the original aim to assess the thermal stability of aluminium-oxygen-

diamond terminations, but this turned out not to be feasible due to problems encountered in producing the aluminium-oxygen terminated diamond.

Lastly, the hierarchical method was applied to diamond to calculate its band gap using DFT.

The results are divided into three sections. The first section describes the development of an aluminium-oxygen termination and includes the characterisation of diamond thin films on silicon substrates. The second section describes thermionic emission studies and includes the characterisation of diamond thin films on molybdenum substrates and the comparison of thermionic emission from three different diamond terminations. The final section describes the computational aspects and the results of applying the hierarchical method to diamond.

3.1 Development of an Aluminium-Oxygen Termination of Diamond

Polycrystalline diamond thin films grown by hot filament CVD on a silicon substrate were used in the development of a method for aluminium-oxygen-diamond termination. These films were first analysed for their quality using SEM and Raman spectroscopy. In Figure 15 (a) it can be seen in that the deposition has been successful in producing a continuous microcrystalline diamond film for sample DFSi 1. By inspecting Figure 16 (a) this fact is further confirmed by the characteristic diamond peak at $\sim 1332\text{ cm}^{-1}$ in the Raman spectrum, although the broad peak between 1400 and 1500 cm^{-1} was also observed and is indicative of amorphous and graphitic carbon which can be deposited at grain boundaries during CVD^{87,88}. Such impurities can alter the mechanical properties of the grown diamond as well as changing its electrical and optical properties^{89,90}. Whilst the graphitic carbon peak appears to be rather large it is worth noting that the Raman spectroscopy carried out here used an excitation wavelength of 514 nm which will give preference to sp^2 carbon atoms over sp^3 atoms thus enhancing the graphitic signal⁸⁸. Taking this into consideration the diamond grown was deemed to be of sufficient quality for the subsequent investigations.

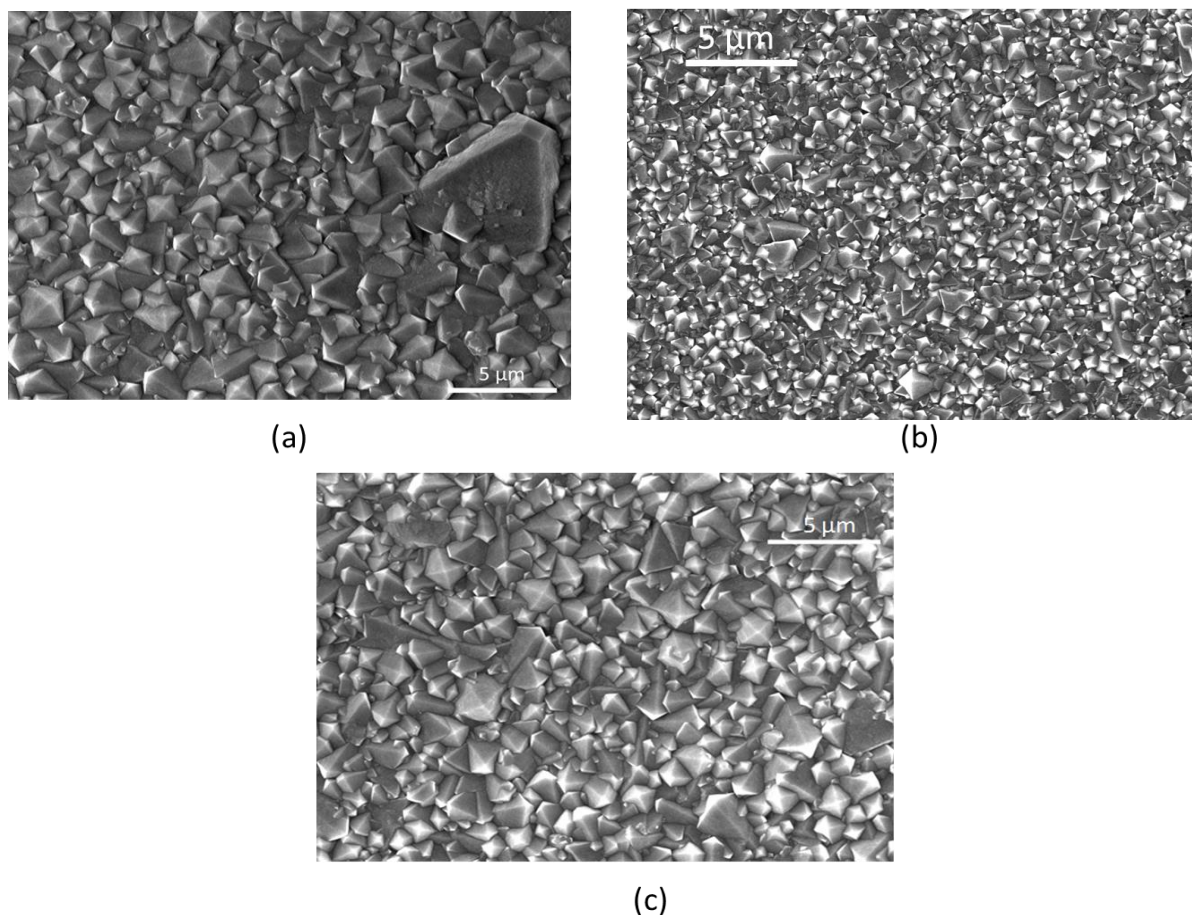


Figure 15: Electron micrographs of diamonds prepared on a silicon substrate.

DFSi 1 (a), DFSi 2 (b), and DFSi 3 (c). Images were taken using a JEOL JSM-I300 instrument.

The same conclusions was drawn for the DFSi 2 (Figure 15 (b) and Figure 16 (b)) and DFSi 3 (Figure 15 (c) and Figure 16 (c)) thin films, which both looked very similar to DFSi 1 in terms of their surface morphology and Raman spectra. Subsequent diamond films grown in the same manner (DFSi 4 and 5) were characterised only by Raman spectroscopy (Figure 16 (d) and (e)); both of these films had a higher peak intensity at $\sim 1332\text{ cm}^{-1}$ relative to the $1400\text{ -}1500\text{ cm}^{-1}$ region, indicating they had a higher ratio of sp^3 hybridised carbon to sp^2 carbon than DFSi 1-3.

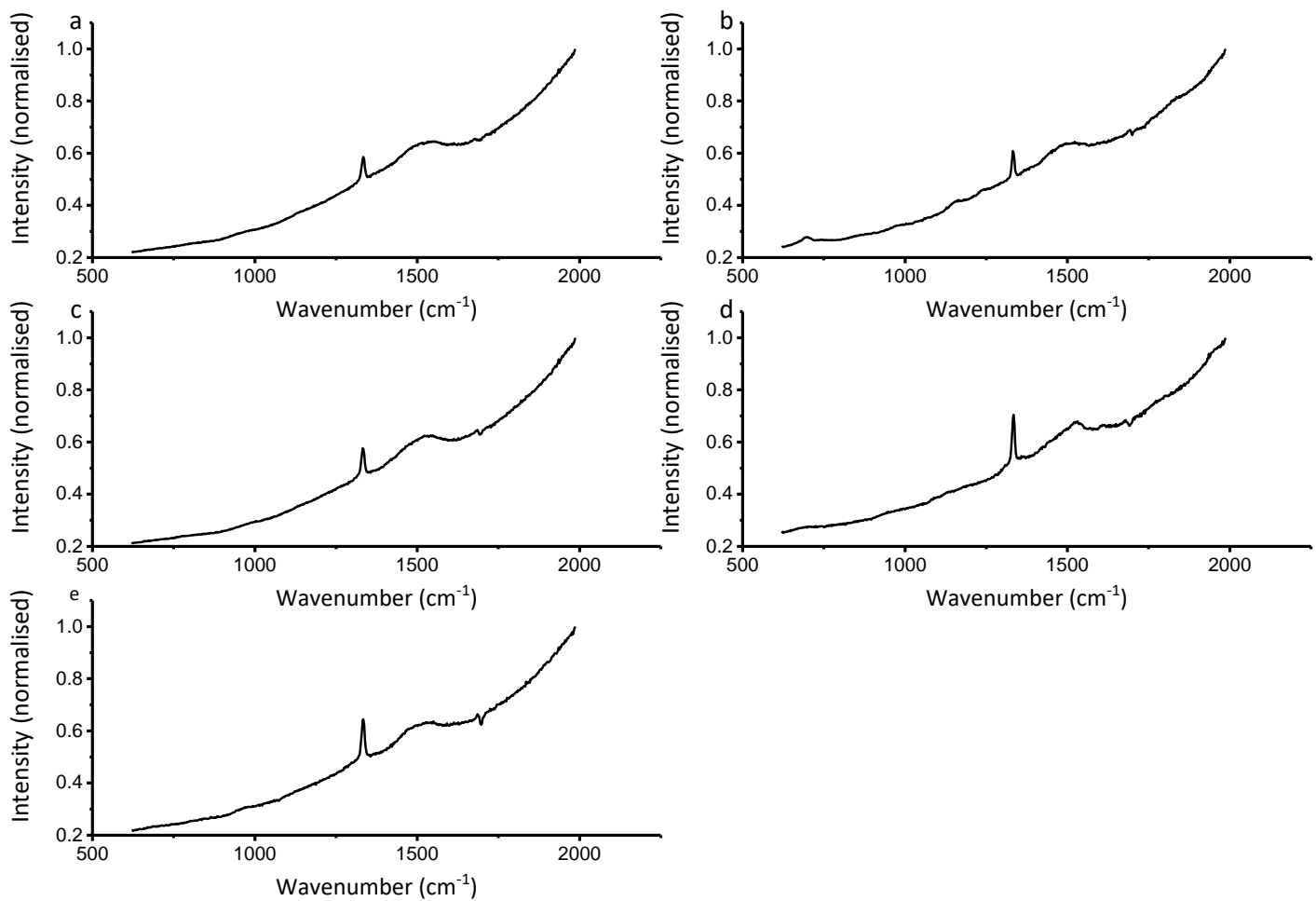


Figure 16: Raman spectra of (a) DFSi 1, (b) DFSi 2, (c) DFSi 3, (d) DFSi 4, and (e) DFSi 5.

All five films were then used in the development of a method to aluminium-oxygen terminate the diamond. SEM was used to determine if any change had occurred in the diamond morphology during the aluminium deposition and etching processes, whilst XPS and EDX were used to determine the surface composition and ensure the diamond had been successfully aluminium-oxygen terminated.

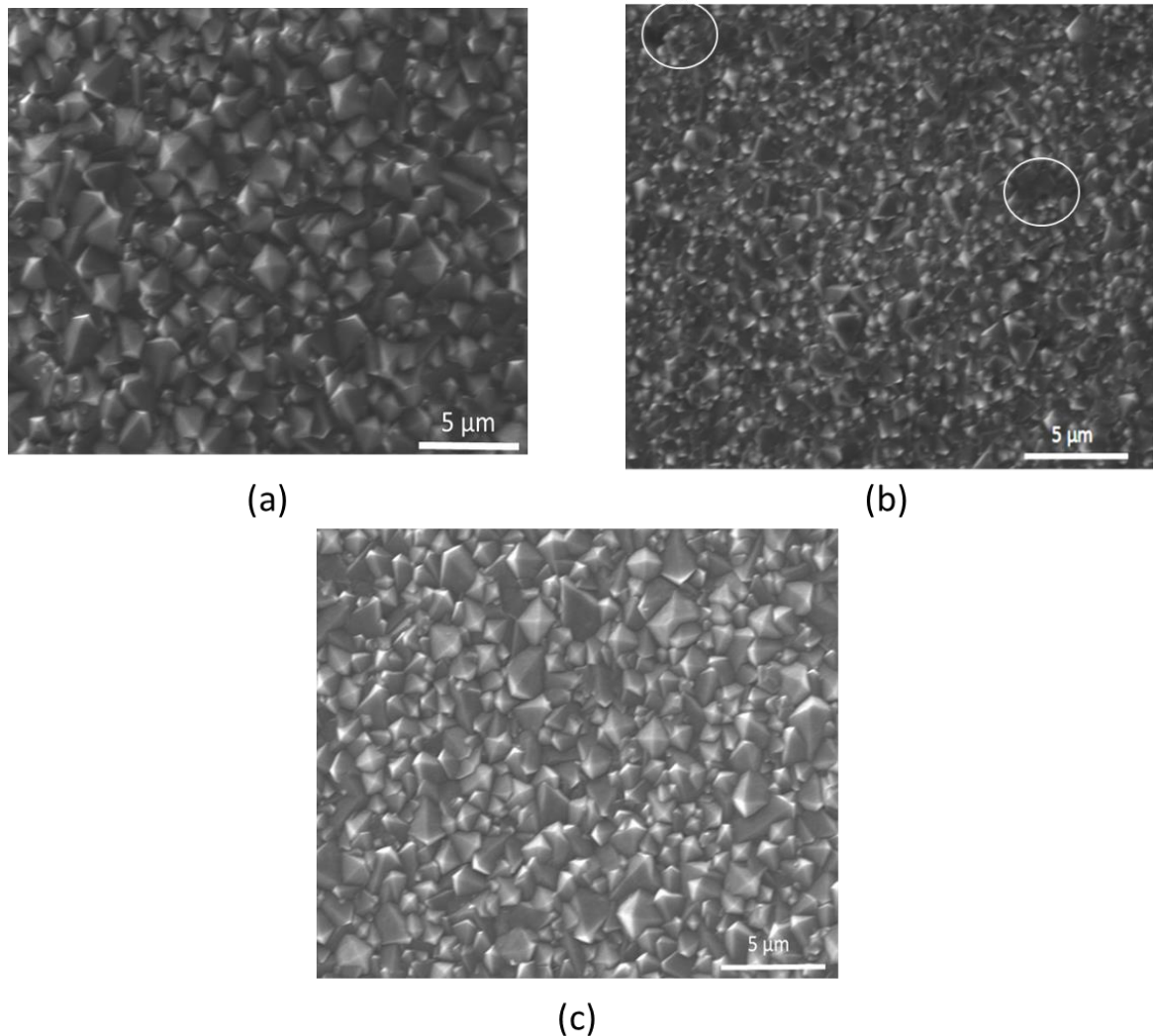


Figure 17: Effect of oxygen termination, aluminium deposition and acid etching on the morphology of diamond. (a) 3h wet etching - DFSi 1; (b) 1h wet etching - DFSi 2; (c) no acid etching - DFSi 3. SEM images were taken after expected deposition of a 12nm thick layer of aluminium using a JEOL JSM-I300 instrument. Circles indicate some regions of proposed altered morphology.

The aluminium coating and etching for 3 h had no effect on the morphology of sample DFSi 1 (Figure 17 (a) compared to Figure 15 (a)). However, there did appear to be some change to the morphology after etching sample DFSi 2 for 1 h, as the diamond facets were much less well-defined (Figure 17 (b)) compared to the unmodified sample (Figure 15 (b)). Differences in the image contrast for Figure 17 (b) could be due a decrease in charging effects resulting from the presence of a layer of conducting aluminium. However, the differences are subtle and may also be due to day-to-day variation in the

SEM. No change in morphology was observed for an unetched sample of oxygen-terminated aluminum-coated diamond (sample DFSi 3; comparing Figure 15 (c) to Figure 17 (c)). Analysis of the sample samples using EDX did not reveal the presence of either aluminium or oxygen, showing that all of them were essentially 100% carbon (Figure 18). The small proportions of nickel and phosphorus observed are not significant and are likely to be a misinterpretation of noise by the software.

However, as EDX is not a particularly surface-sensitive technique it would be unlikely to detect small

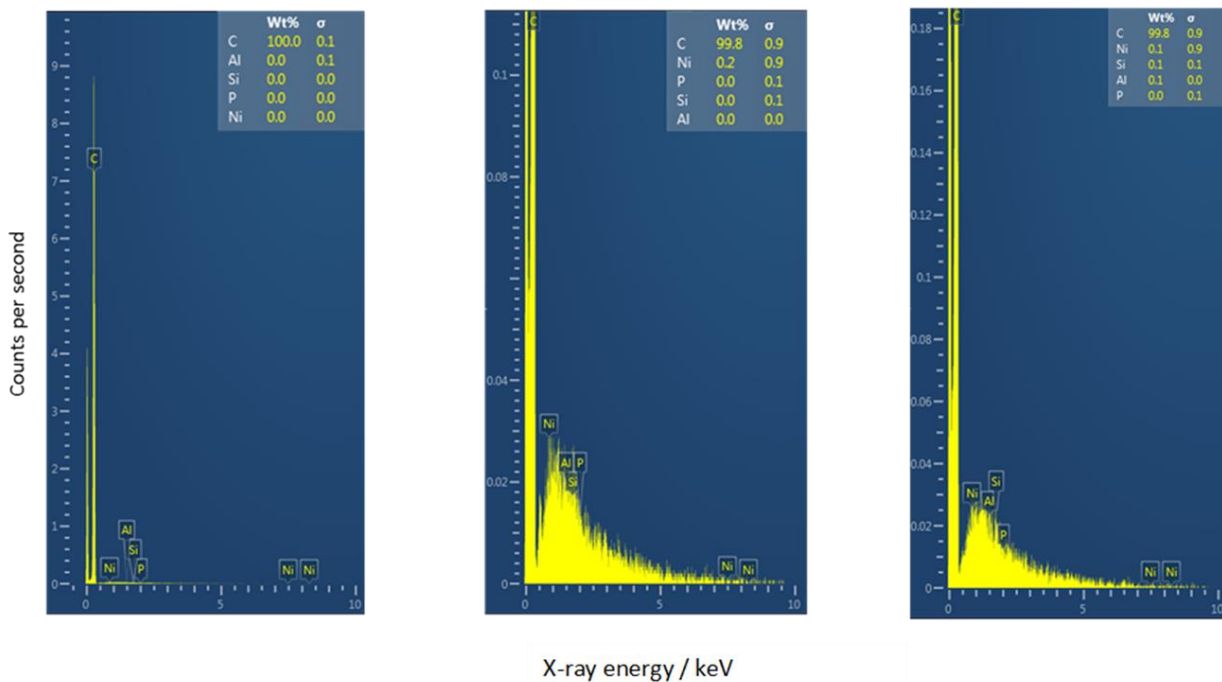


Figure 18: Effect of oxygen termination, aluminium deposition and acid etching on EDX spectra of different diamond samples. Left - DFSi 1 after aluminium deposition and etching; Middle - DFSi 2 after aluminium deposition of ~12 nm and etching; Right - DFSi 3 after aluminium deposition.

amounts of aluminium or oxygen lying on the diamond surface. In order to gain a better understanding of the surface composition, a more surface-sensitive method, XPS was carried out on DFSi 1 (Figure 19) and DFSi 3 (Figure 20). Using the largest peak area for each element in the XPS spectrum, the relative abundance of different elements present on the surface could be calculated. Analysis of DFSi 1 (Figure 19 (a)) using this method demonstrated the presence of both oxygen (13.06%) and a trace of aluminium (0.19%). These results confirm that the diamond surface was oxygen terminated and that a small amount of aluminium was present even after etching for 3 h. Nitrogen was also present as an adsorbed species on the surface of the diamond. As a consequence of this observation it was decided to heat the samples in UHV to 300°C for 30 min to degas the surface prior to XPS analysis. Such an anneal has been previously shown to successfully remove adsorbed contaminants⁶². The XPS

spectrum of DFSi 1 after this anneal (Figure 19 (b)) showed a reduction in the concentration of nitrogen on the surface from 1.9 to 0.32%. This treatment also significantly reduced the concentration of oxygen from 13.06 to 5.42%. It is likely that the desorbed oxygen was water and oxygen from the air and the remaining oxygen is the termination induced by exposure to plasma.

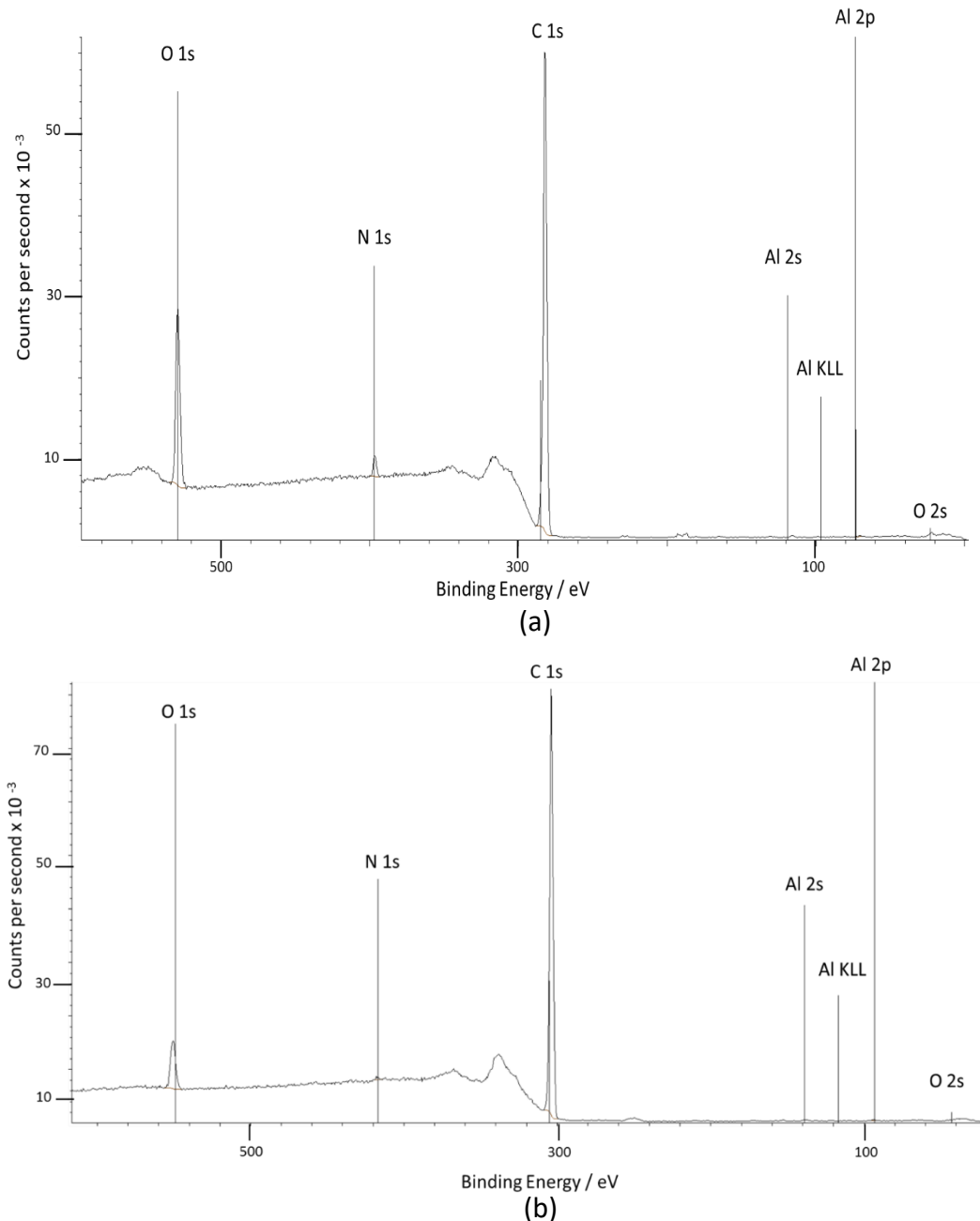


Figure 19: XPS spectra of DFSi 1 (a) oxygen termination, aluminium deposition of ~12 nm and etching and (b) oxygen termination, aluminium deposition of ~12 nm and etching, and a 300°C anneal in UHV. The atomic concentration is as follows: (a) 13.06% oxygen, 84.85% carbon, 1.9% nitrogen, and 0.19% aluminium. (b) oxygen 5.42%, carbon 93.85%, nitrogen 0.32%, and aluminium 0.41%.

In the case of DFSi 3 no aluminium was detected (Figure 20) which was unexpected given the lack of etching. On the basis of this observation, and the difference in morphology change, it was decided that depositing such a thin layer of aluminium using this method and then etching it, was unreliable. The peaks in these spectra were all shifted higher in energy than expected and this is likely a result of charging, a well known issue with carrying out XPS on an insulator^{91,92}. As a consequence further XPS analysis of DFSi 2 was deemed unnecessary.

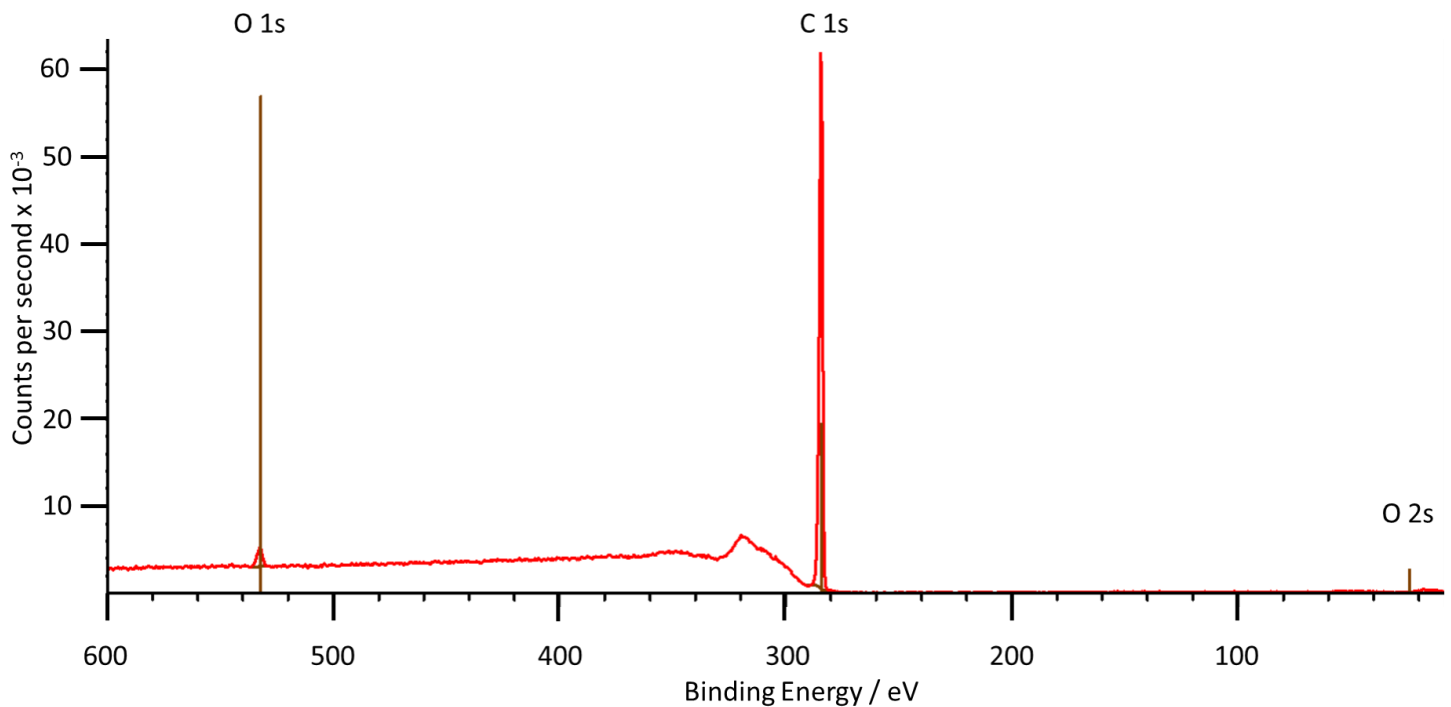


Figure 20: XPS spectrum of DFSi 3 after aluminium deposition of ~12 nm and a 300°C degassing anneal in UHV. The atomic concentrations were as follows: oxygen 1.7%, and carbon 98.3%.

In order to ensure a total and even coverage of aluminium over the diamond thin film and to give a larger margin for error during the etching procedure, a more faithful recreation of O'Donnell *et al*'s "thick film" method^{50,57,62} was used. This deposits a ~100 nm layer of aluminium onto the diamond surface. SEM images of DFSi 4 and 5, modified in this way, showed the presence of patches of material with a dark contrast lying over and between the polycrystalline diamond (circled in Figure 21). It appears as though the aluminium has filled in the gaps between the diamond crystal facets, while the facets themselves appear less well-defined compared to the surfaces of polycrystalline diamonds grown in the same manner (c.f. Figure 15).

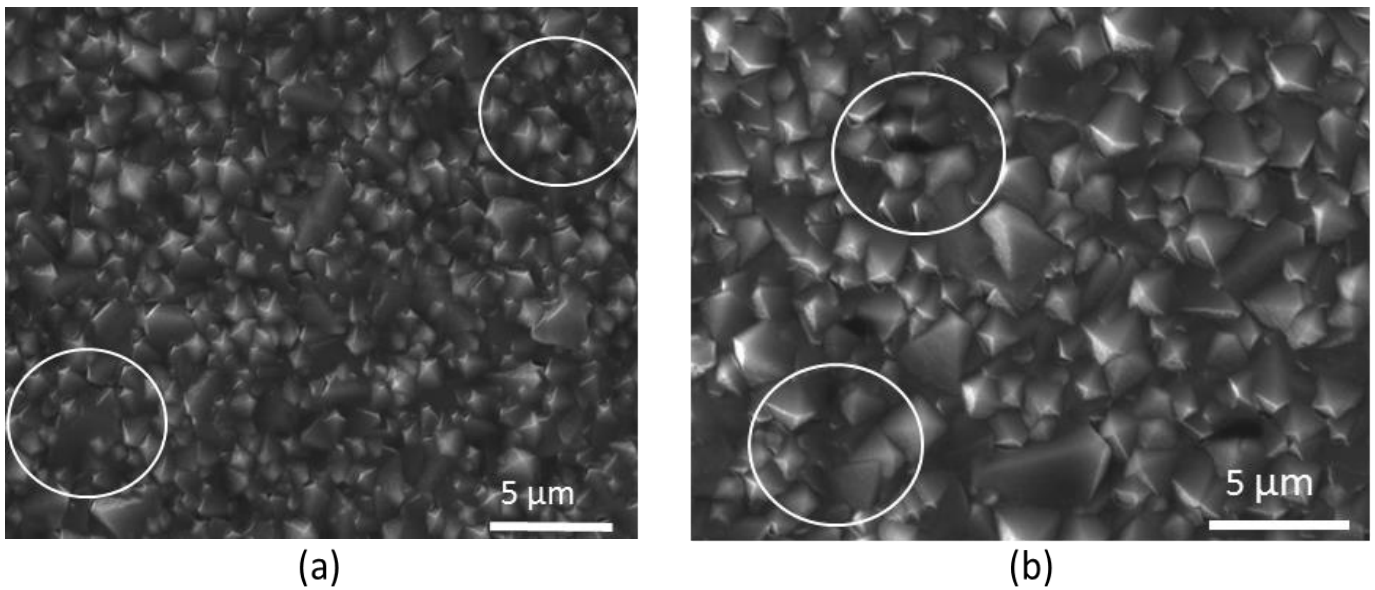


Figure 21: Effect of depositing a thick ~100 nm layer of aluminium on diamond. Electron micrographs of DFSi 4i (a) and DFSi 5 (b) after oxygen termination and aluminium deposition of ~100 nm. Circles indicate some regions of proposed altered morphology.

The presence of aluminium was further confirmed by EDX (Figure 22). These results also suggested that zinc was present in the film; the source of this is unknown although it seems likely to have been introduced during the aluminium deposition as there are zinc components of the bell jar evaporator. In order to gain more information on this, DFSi 4 was split into two (henceforth known as DFSi 4i and DFSi 4ii) and XPS was carried out on DFSi 4i after a degassing anneal. These results indicated that the zinc concentration on the surface was negligible and the concentration of oxygen was extremely high. It seems likely that the large percentage of oxygen is a result of the aluminium layer oxidising whilst the sample was out of vacuum. This spectrum is unlikely to give much information on the diamond-aluminium interface as a thick layer of aluminium had been deposited and XPS is only sensitive to atoms within tens of nm of the surface. Thus, the XPS spectrum is likely to be of the aluminium surface coating only, which is consistent with the very low carbon content observed. Trace quantities of silicon are likely present due to washing of the sample in glasswear.

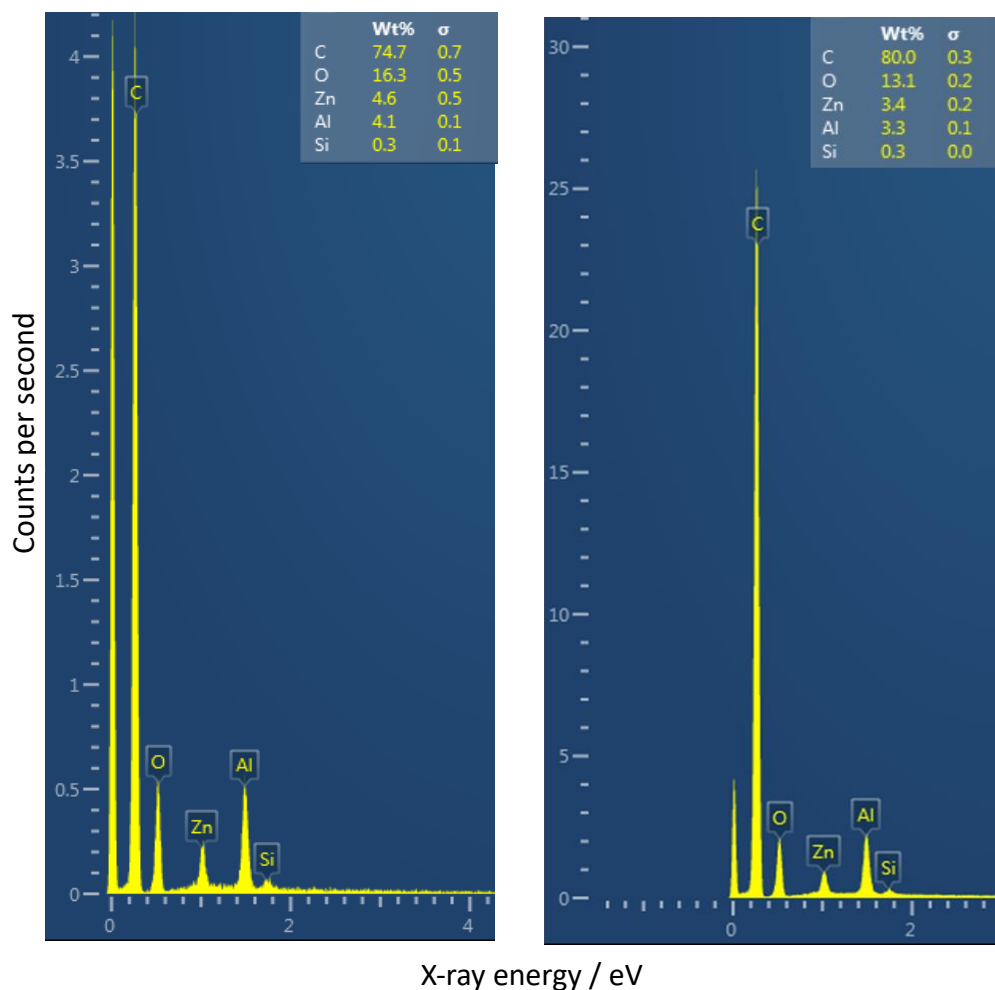


Figure 22: EDX results for DFSi 4i (left) and DFSi 3 (right) after oxygen termination and deposition

Subsequently DFSi 5 was etched with 1.2 M HCl for 1 h whilst a portion of DFSi 4i was etched for 3 h. XPS analysis of these samples (Figure 23 and Figure 25) demonstrated the presence of aluminium in the quantities found on the surface of DFSi 1 and 2. The similarity of these results implies that there is a population of aluminium which is strongly bonded to the diamond-oxygen surface and will not be removed by the etching conditions employed in this study. As a result of this, a 1 h etch was deemed sufficient to remove excess aluminium which was not bonded to the diamond surface.

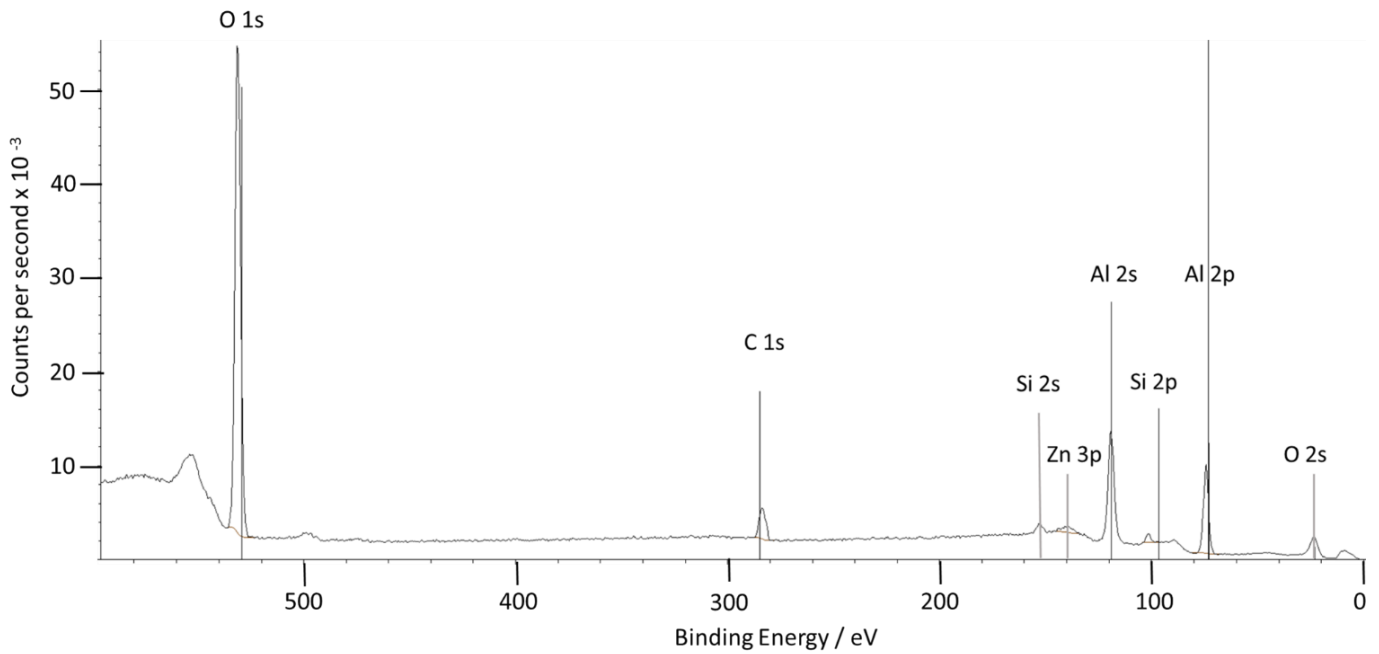


Figure 24: XPS spectrum of DFSi 4i after oxygen termination, aluminium deposition of ~100 nm (with no etch), and a 300°C degassing anneal in UHV. The atomic concentrations are as follows: oxygen 49.8%, carbon 10.54%, silicon 1.85%, aluminium 34.68%, and zinc 3.12%.

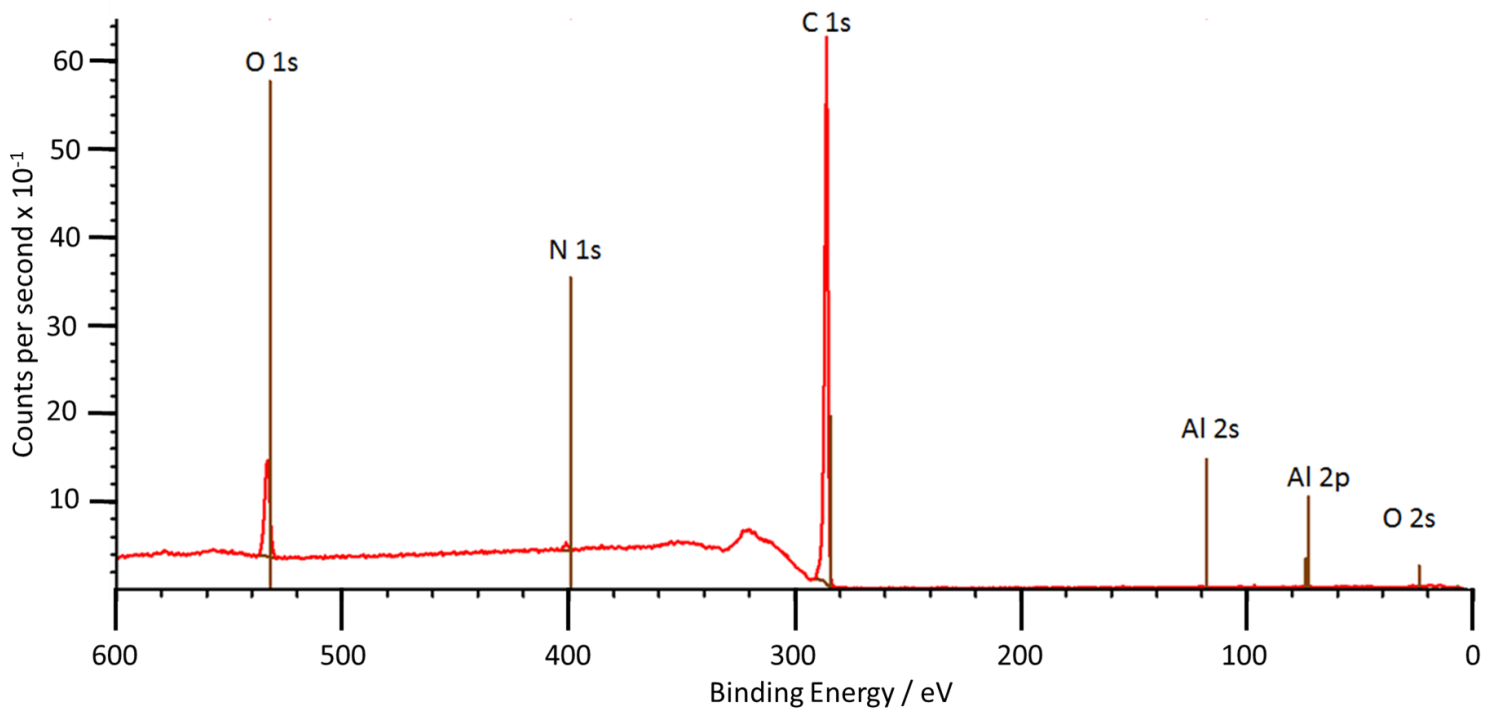


Figure 23: XPS spectrum of DFSi 4i after oxygen termination, aluminium deposition of ~100 nm, a 3 h wet etch, and a 300°C degassing anneal. The atomic concentrations are as follow: oxygen 7.86%, carbon 91.08%, nitrogen 0.77%, and aluminium 0.28%.

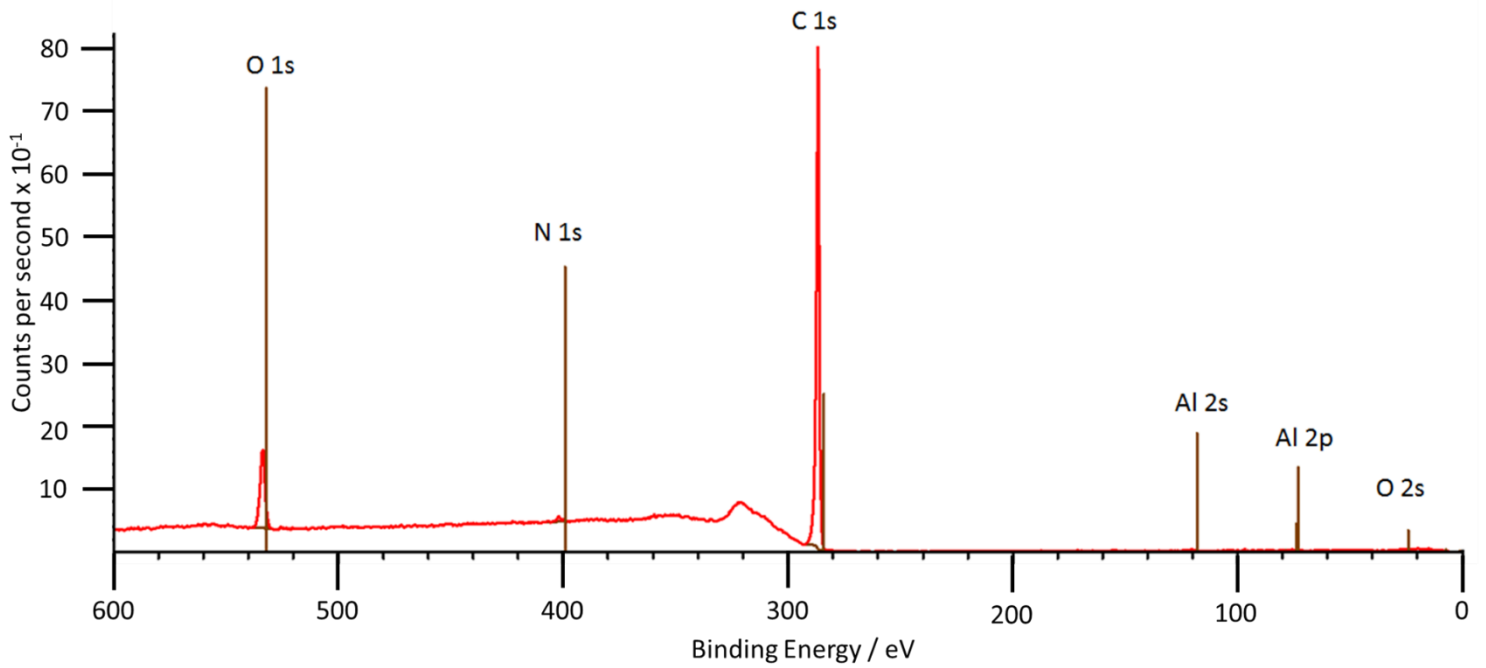


Figure 25: XPS spectrum of DFSi 5 after oxygen termination, aluminium deposition of ~100 nm, a 1 h wet etch, and a 300°C degassing anneal. The atomic concentrations are as follows: oxygen 7.38%, carbon 91.79%, nitrogen 0.52%, and aluminium 0.30%.

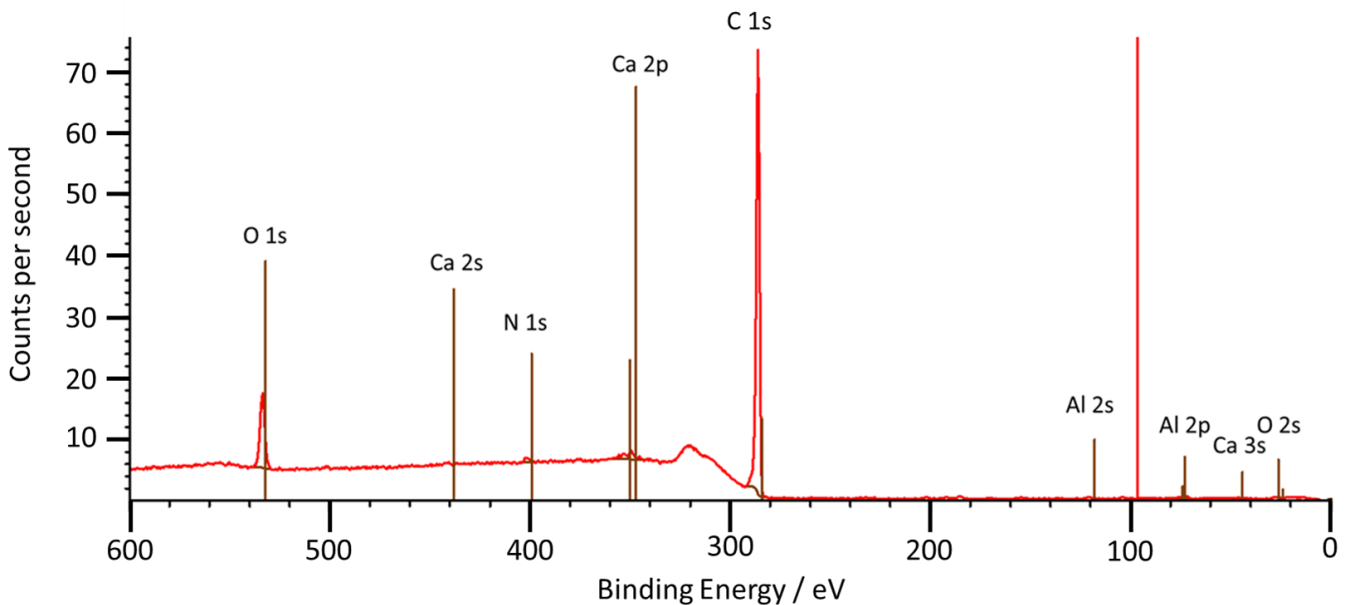


Figure 26: XPS spectrum of DFSi 4ii after oxygen termination, aluminium deposition, a 1 h wet etch, and a 300°C degassing anneal. The atomic concentrations were as follows: oxygen 7.21%, carbon 89.04%, nitrogen 0.73%, aluminium 2.06%, and calcium 0.97%.

To increase the proportion of aluminium tightly bonded to the diamond surface, the effect of heating prior to etching was investigated. This might promote bond formation between aluminium and the oxygen-terminated diamond by providing the energy required to overcome any kinetic barrier to bonding. XPS analysis of DFSi 4ii which had been annealed under UHV at 500°C for 10 mins before being wet etched in 1.2 M HCl for 1 h (Figure 26) showed an increase in the proportion of surface-bound aluminium compared to DFSi 5 which had not been treated in this way.

The shape and position of the Al 2p peak in the XPS spectrum is characteristic of the nature of the interaction between the diamond and aluminium and was used to further define the nature of the surface modifications. When a sample of “thick” aluminium-coated diamond was analysed without being etched (DFSi 4ii; Figure 28) a single peak with a maximum binding energy of around 78 eV was observed. This is diagnostic of aluminium oxide⁹³. Detection of mainly aluminium oxide is not surprising; the sample was exposed to air so aluminium oxide formation on the metal surface is likely given aluminium’s propensity to form oxides⁹⁴. The thickness of the aluminium layer would result in little else being detected using XPS, as discussed earlier.

By studying the position and shape of the Al 2p peak of DFSi 5 (Figure 27), an understanding of the nature of the aluminium present after etching can be obtained. This peak has a lower maximum binding energy of just over 75 eV and a much more asymmetric shape. This asymmetry is indicative of multiple aluminium environments being present, and by peak fitting it is possible to infer the nature and relative proportions of these different environments. Such peak fitting resulted in two different aluminium environments being found to be present after etching. Most of the aluminium is present at a lower binding energy than the oxide seen in Figure 28. From the literature⁹⁴, it seems likely that this is the oxycarbide – *i.e.* aluminium bonded to carbon via a bridging oxygen. This environment is the desired configuration as it is analogous to how the other light metals have interacted with the oxygen-diamond surface to induce a NEA^{26,50,57,62,76}. There is a second environment present at higher energy and in a lower proportion which is proposed to be residual aluminium oxide. Although the peak maximum does not correspond exactly to 78 eV, as in Figure 28, these are small signals with a large amount of noise so a small discrepancy when applying statistical methods to peak fit is not surprising.

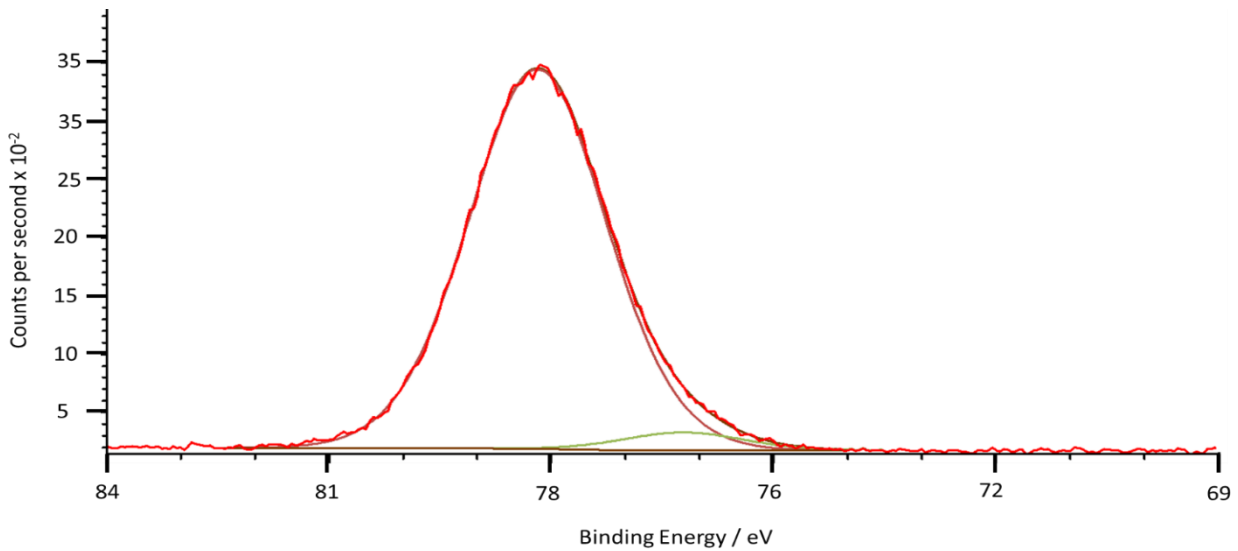


Figure 28: Al 2p peak from XPS spectral analysis of DFSi 4ii after oxygen termination, aluminium deposition of 100 nm, and a 300°C degassing anneal. Red line – XPS spectral peak; dull red line and green line represent fitted peaks.

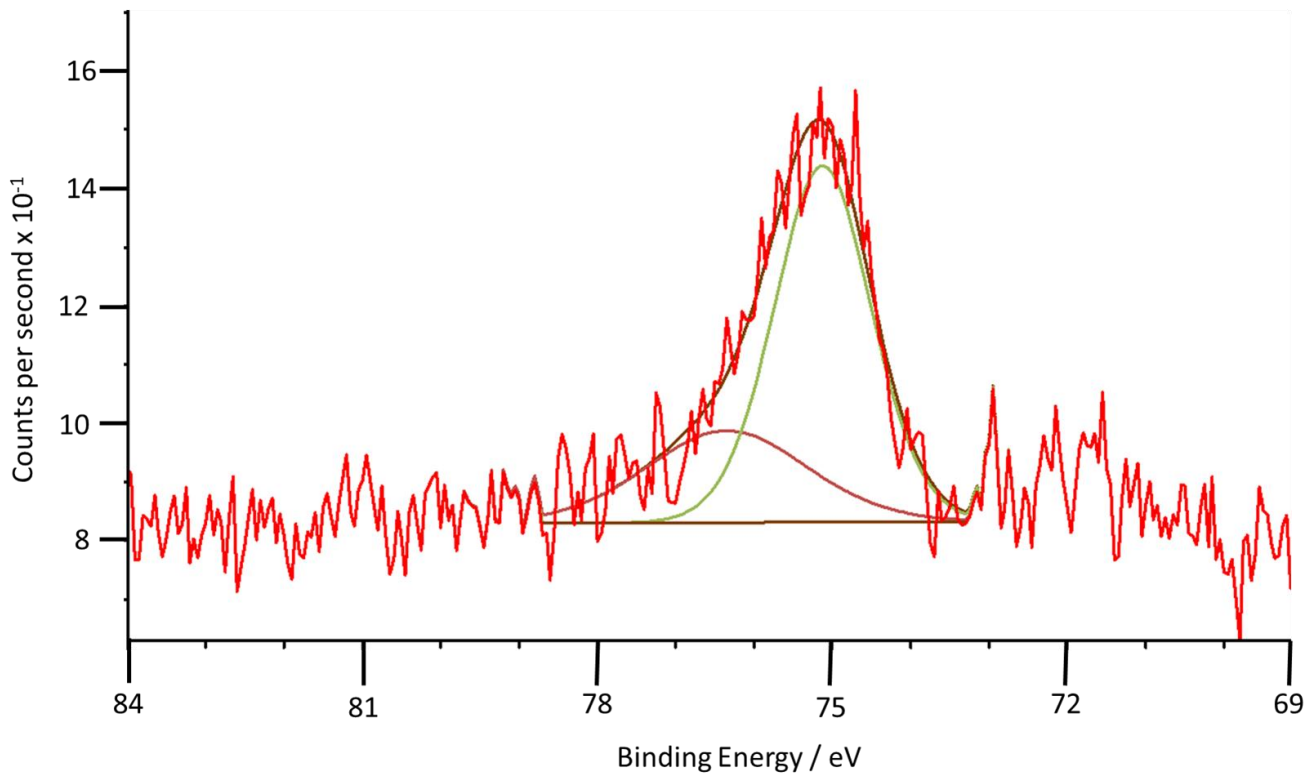


Figure 27: Al 2p peak from XPS spectral analysis of DFSi 5 after oxygen termination, aluminium deposition of 100 nm, a one hour wet etch, and a 300°C degassing anneal. Red line – XPS spectral peak; dull red line and green line represent fitted peaks.

The effect of heating on the nature of the aluminium-diamond interface can be seen in the Al 2p peak of DFSi 4ii after heating and etching (Figure 29). In this, two distinct peaks are present in similar proportions. These two peaks can be assigned to the oxycarbide at approximately 76 eV and the carbide at around 72 eV. This would suggest that heating the sample encourages the displacement of

oxygen by aluminium at the diamond surface to react directly with carbon. Whether such a bonding arrangement will result in a stable NEA is unknown, however previous work would suggest it is not the ideal termination electron emission^{26,50,51}.

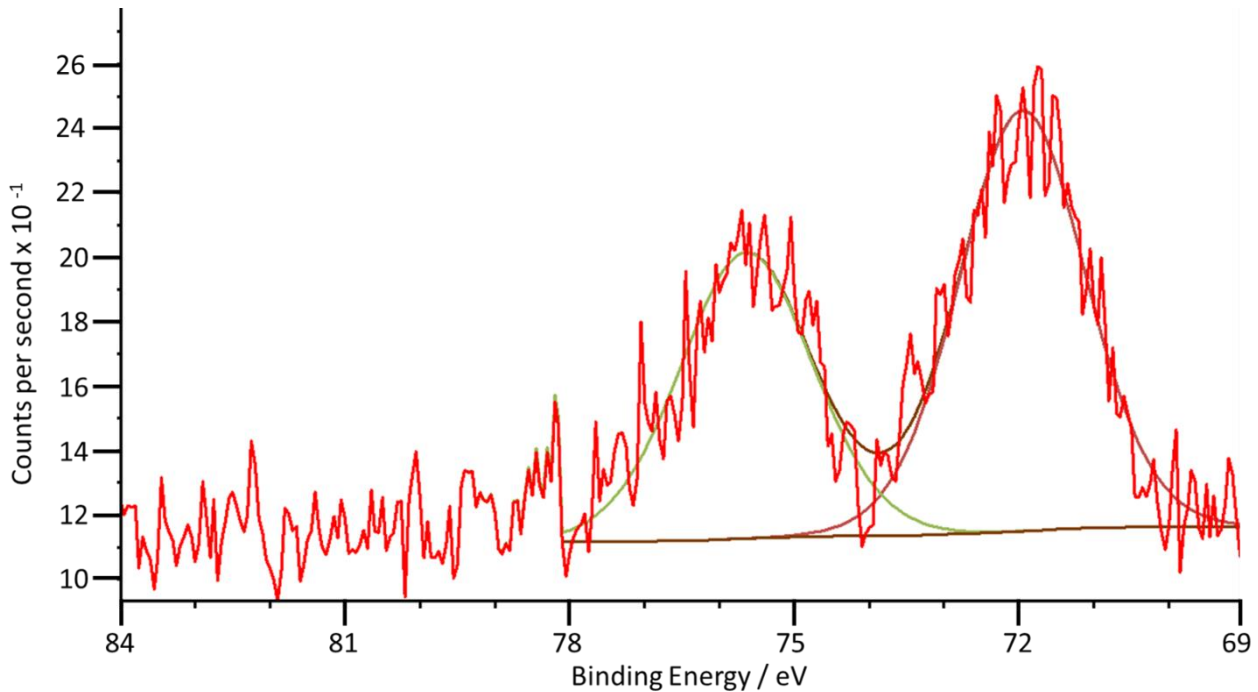
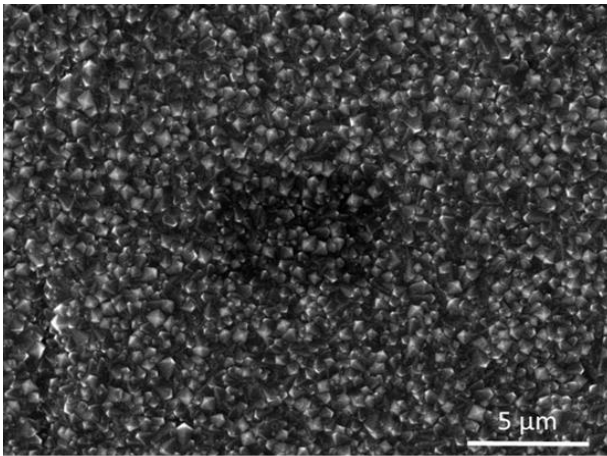


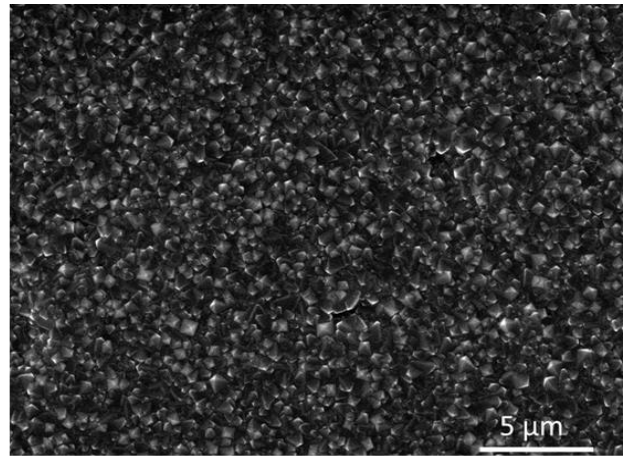
Figure 29: Al 2p peak from XPS spectral analysis of DFSi 5 after oxygen termination, aluminium deposition of 100 nm, a 500°C anneal, a 1 h wet etch, and a 300°C degassing anneal. Red line – XPS spectral peak; dull red line and green line represent fitted peaks. XPS spectrum of the aluminium 2p peak of

3.2 Thermionic Emission

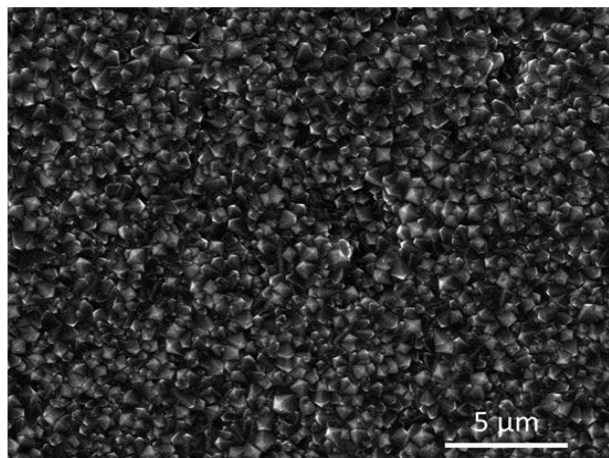
Thermionic emission experiments were carried out on nitrogen-doped polycrystalline diamond films grown by microwave plasma CVD on molybdenum substrates. Figure 30 and Figure 31 were used to characterise the purity and nature of these films. In all cases we can see that a continuous film of diamond has been grown but these films are quite different to the undoped diamond films grown by HFCVD. Importantly, these films are nanocrystalline diamond rather than microcrystalline diamond, which is not surprising as the inclusion of nitrogen is known to result in smaller crystals^{82,96}. The peaks in the Raman spectra can be assigned to the same carbon environments as above, and in all cases the diamond film was deemed pure enough.



(a)



(b)



(c)

Figure 30: Electron micrographs of DFMo 1 (a), DFMo 2 (b), and DFMo 3 (c).

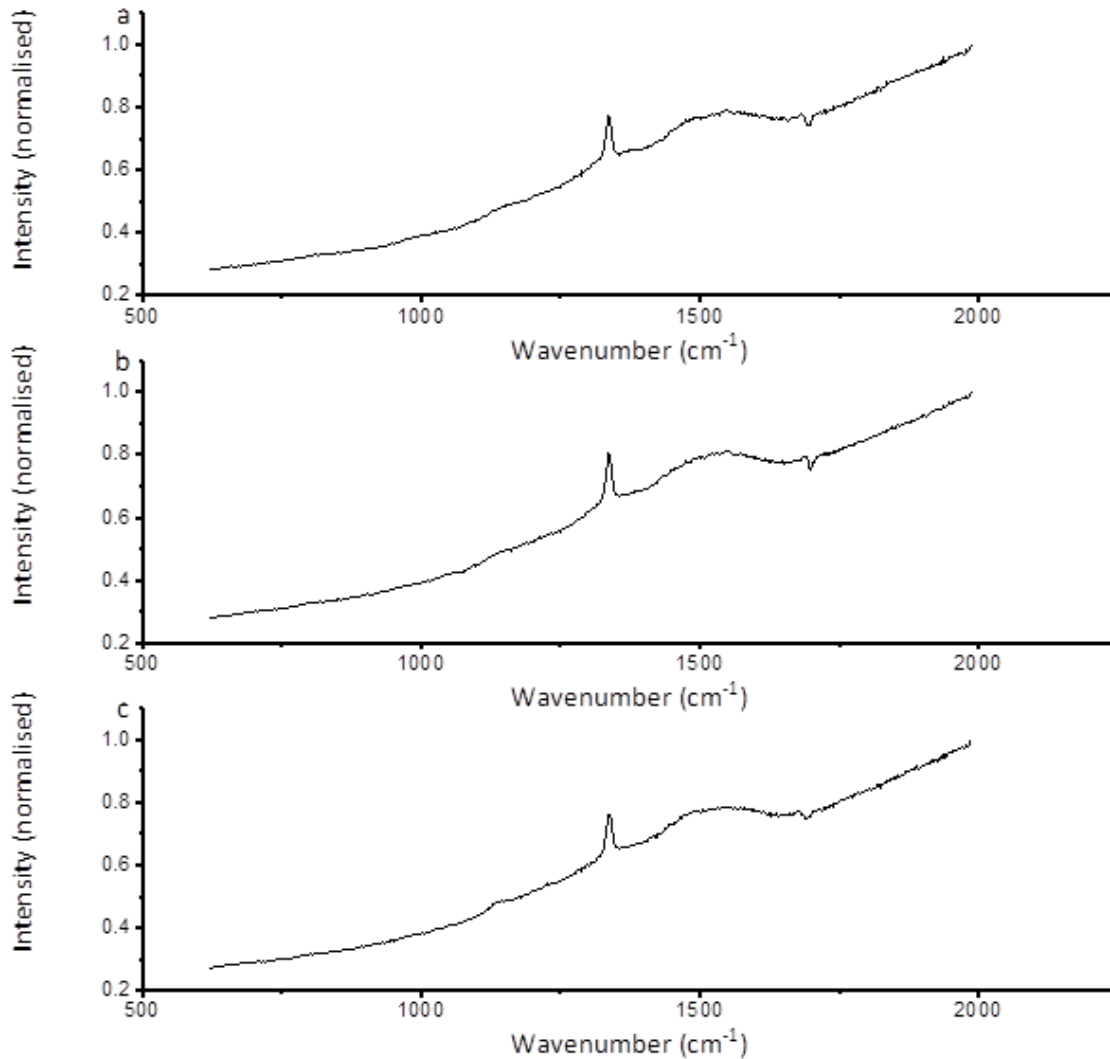


Figure 31: Raman spectra of (a) DFMo 1, (b) DFMo 2, and (c) DFMo 3.

Once the purity of these films was determined, each sample was terminated with either hydrogen, oxygen, or aluminium-oxygen and the thermionic emission was measured. DFMo 1 was an oxygen-terminated sample and was not expected to have any thermionic emission as it is well known that oxygen terminations give a positive electron affinity. Figure 33 (a) shows there is essentially negligible thermionic current from this sample which does not vary with temperature. DFMo 2, in contrast, was hydrogen-terminated which should have a NEA. As such, a large thermionic current was expected, and this is what was observed (Figure 33 (b)). DFMo 3 was treated in the same manner as DFSi 5 before thermionic emission experiments were carried out in order to see if this level of aluminium was sufficient to result in a lowering of the work function and an increase in thermionic emission. As can be seen from Figure 33 (c) no thermionic emission was observed and the results were almost identical to DFMo 1. It seems likely that either the level of aluminum was too little or that there was a problem in the diamond film grown. To identify which of these were the issue, DFMo 2 was oxygen

terminated and a thick layer of aluminium was deposited onto the surface. DFMo 2 was used as it has already been shown that this diamond sample exhibited thermionic emission when the correct surface dipole is present. A much shorter etch (10 mins) was carried out in an attempt to increase the aluminium concentration. It is important to note here that upon visual inspection the sample surface was not homogenous. An aluminium deposition has been seen to give a darkening of the surface in earlier experiments but, after this 10 min etch, the colour of the surface was inconsistent and it seems likely this is due to different thicknesses of aluminium being present across the surface (Figure 32). In any case, no thermionic emission was observed.



Figure 32: Photograph of DFMo 2 after oxygen termination, aluminium deposition and a 10 min wet etch with 1.2 M HCl. The patches that are lighter are indicative of a thinner aluminium coating.

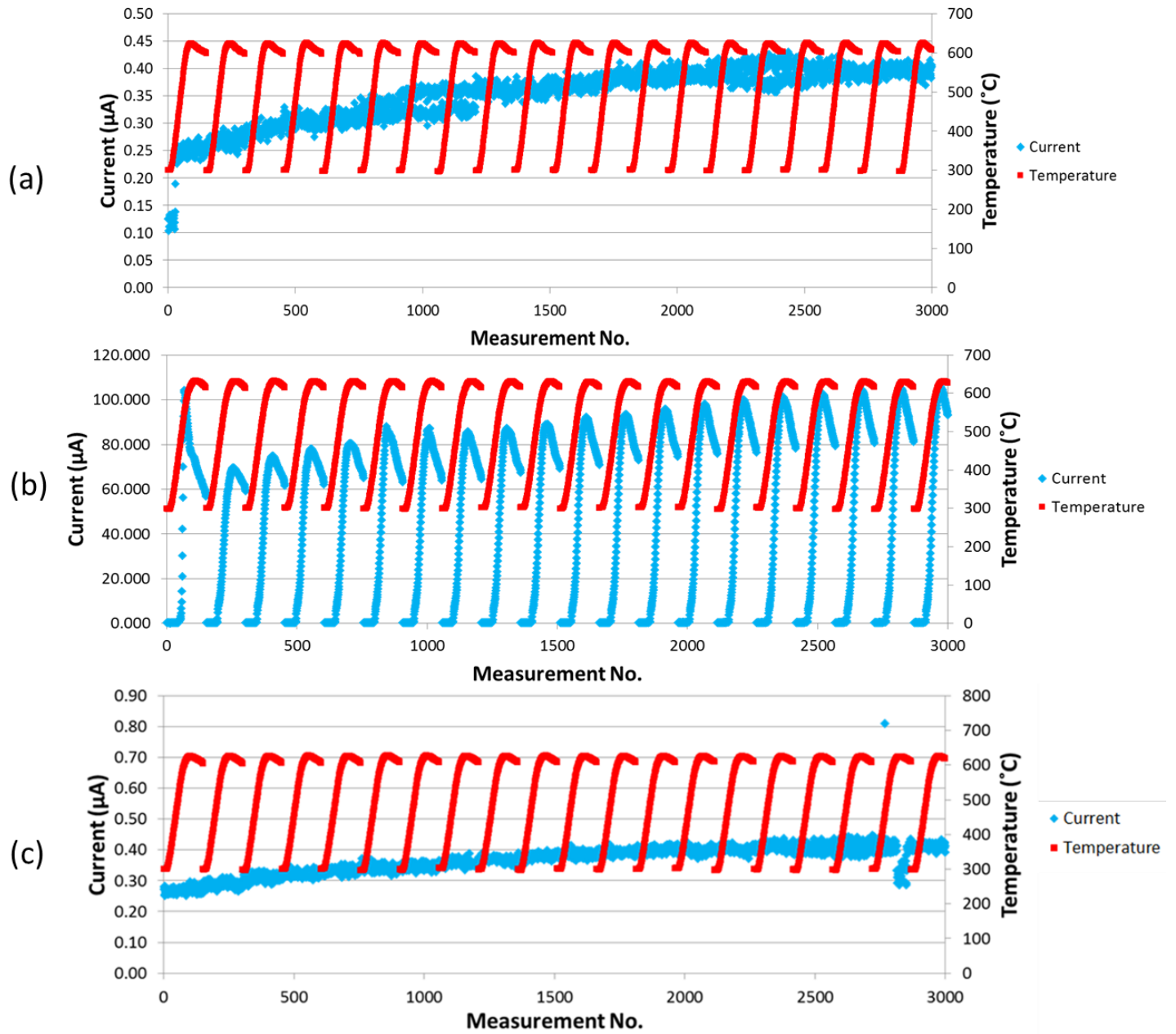


Figure 33: Thermionic emission results for (a) DFMo 1 after oxygen termination, (b) DFMo 2 after hydrogen termination, and (c) DFMo 3 after oxygen and aluminium termination.

3.3 Computational results

The following work has applied the hierarchical method to modelling diamond to give an accurate method for calculating its band gap. As far as the author is aware, the hierarchical method has not previously been applied to a crystal with an open shell unit cell (*i.e.* requiring terminating groups on the surface) as is the case for diamond. The modelling was initially carried out by building a variety of different shapes and sizes of diamond clusters and classifying each atom into an environment (bulk, one hydrogen, and two hydrogens). It was assumed that all atoms in each environment had constant energy and this could be used to decompose the total energy term into contributions from the sum of all atoms in each environment. By calculating the energy of a variety of different clusters, a set of simultaneous equations were generated and the contribution of the bulk term was found. This was carried out for the neutral clusters as well as cationic clusters (generated by removing one electron from the highest occupied molecular orbital) and anionic clusters (generated by adding one electron to the lowest unoccupied molecular orbital). These charged clusters were used because the difference in energy between them gives an estimate for the band gap. Clusters were built manually using the GaussView package with a carbon-carbon bond length of 1.567 Å (derived from a diamond unit cell with a lattice parameter of 3.5 Å) and a carbon-hydrogen bond length of 1.070 Å. The total energies of these clusters were calculated using the Turbomole package, the B3LYP functional, and the def-SVP basis set. The B3LYP functional was used because this has been used in the past to calculate the band gap of diamond so this allows easier comparison to benchmark results. The def-SVP basis set was used as this was created by the makers of Turbomole and is said to have the same accuracy of the 6-31G basis set⁹⁷.

Total Number of Carbon Atoms	Total Number of Atoms	Number of Bulk Carbons	Number of Carbons with One Hydrogen	Number of Carbons with Two Hydrogens
18	42	1	10	7
26	56	2	18	6
35	71	5	24	6
39	79	8	22	9
43	87	11	20	12
53	101	12	34	7
68	124	18	44	6
84	148	26	52	6

Table 2: The initial clusters used when applying the hierarchical method to diamond and the number of carbons in each environment.

Calculations were carried out for clusters of size ranging between 18 and 84 carbon atoms (Table 2 and Figure 33)). Simultaneous equations were solved using the largest clusters possible for a given maximum cluster size in a method similar to that described by Manby *et al.* for lithium hydride and crystalline neon^{79,81,98}. The calculated bulk energies per atom did not converge

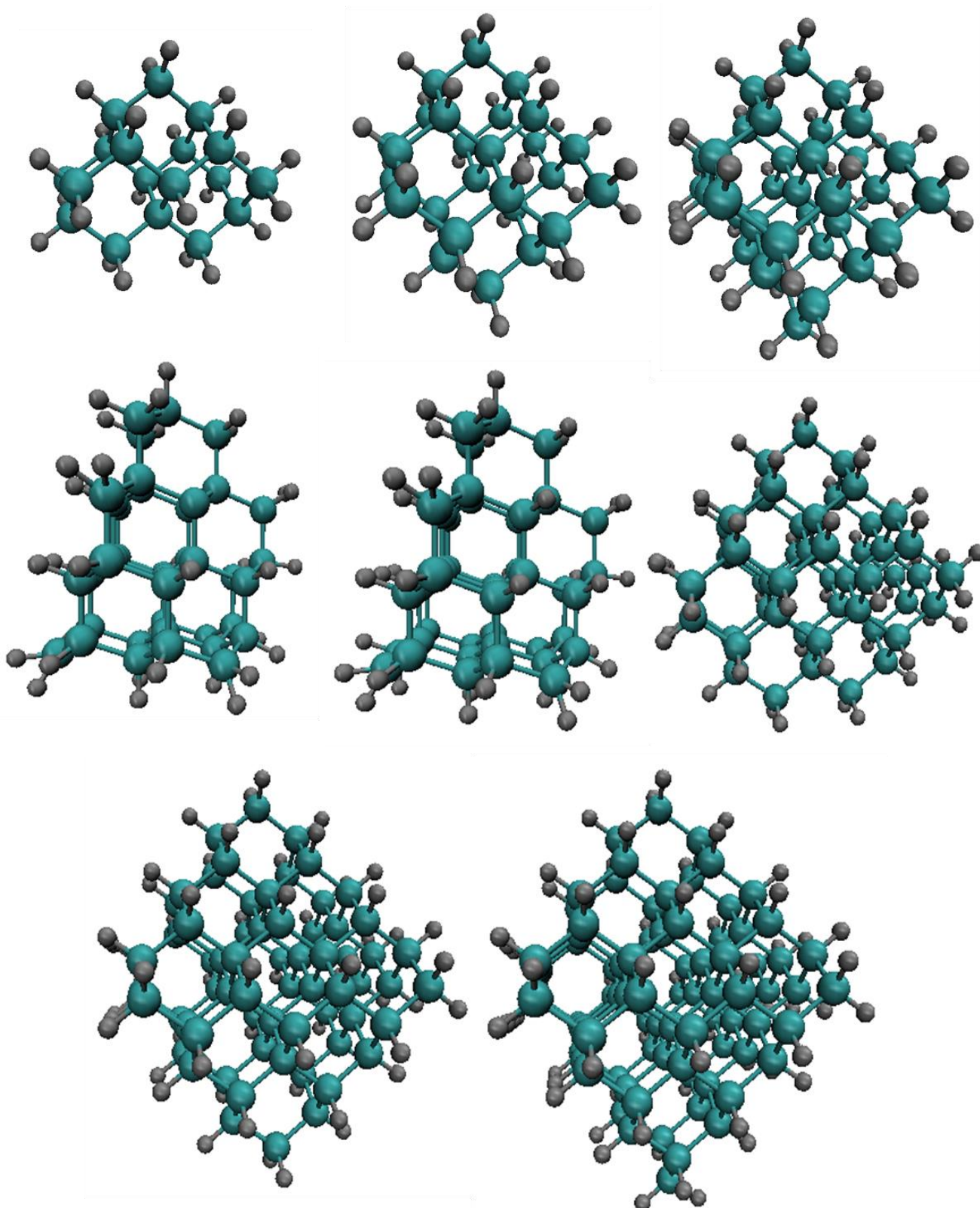


Figure 34: Initial clusters the hierarchical method was applied. From left to right these are the 18-carbon cluster, the 26-carbon cluster, the 35-carbon cluster, the 39-carbon cluster, the 43-carbon cluster, the 47-carbon cluster, the 68-carbon cluster, and the 84-carbon cluster.

with increasing cluster size, particularly for the anionic and cationic clusters (Figure 35 and 36), and the values do not appear to be converging. Instead, they vary quite randomly. One of the main issues with this set of clusters was a lack of systematic growth, as the clusters used here were built in a rather random fashion. Despite this lack of convergence, the band gap was calculated by subtracting the energy per bulk atom of the cationic cluster from that of the anionic cluster, in the hope that any errors would be cancelled out in the subtraction process. However, the values calculated were very poor compared to the experimental value of ~ 5.5 eV⁹⁹. In fact, the calculated band gaps appear to be becoming more inaccurate with larger clusters which is the opposite of what would be expected, with some even giving a negative band gap (Figure 36).

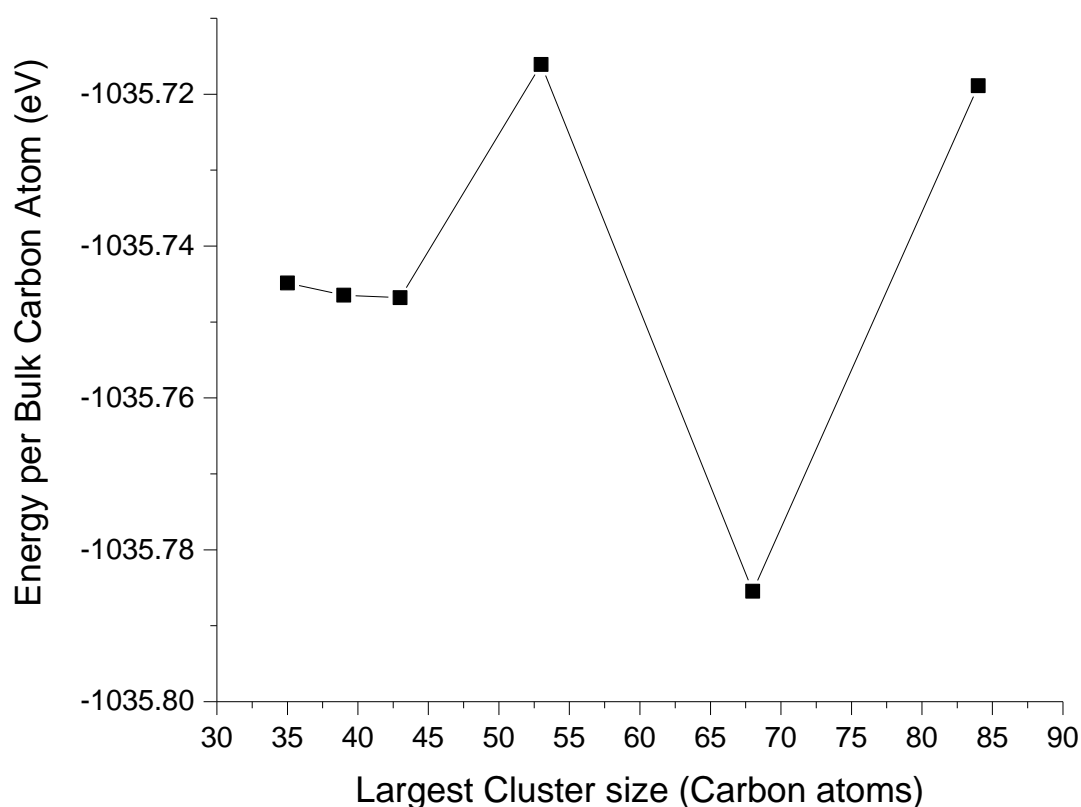


Figure 35: Energy per bulk carbon atom calculated using the hierarchical method with clusters ranging in size from 18-84 carbon atoms.

It was decided to concentrate on generating a set of neutral clusters which converged with respect to the energy per bulk atom. One method which was tried was to build diamond tetrahedra and remove the corners of these clusters one at a time (Figure 37). Whilst this appears to be a systematic method, it yielded sets of linearly dependent simultaneous equations which are insoluble.

The final method attempted was to build a large tetrahedral diamond cluster and generate all the other clusters from this by removing planes of atoms from the bottom upwards (Table 3 and Figure 39). This method yielded a set of linearly independent simultaneous equations which were soluble, and the energies calculated from these clusters appear to converge to a value per bulk atom quickly; the final three values are all within 0.002 eV of one another (Figure 38). The first value is much higher which is probably because it involved the three smallest clusters. As the clusters increase in size the increase in the number of bulk carbons becomes much larger and so any clusters involving the 26-carbon cluster will be much more dominated by surface effects *i.e.* the influence of carbons with one or two hydrogens due to their greater proportions. However, the clusters involved were very large and the largest is already beyond the feasible application of higher levels of theory due to the computational cost.

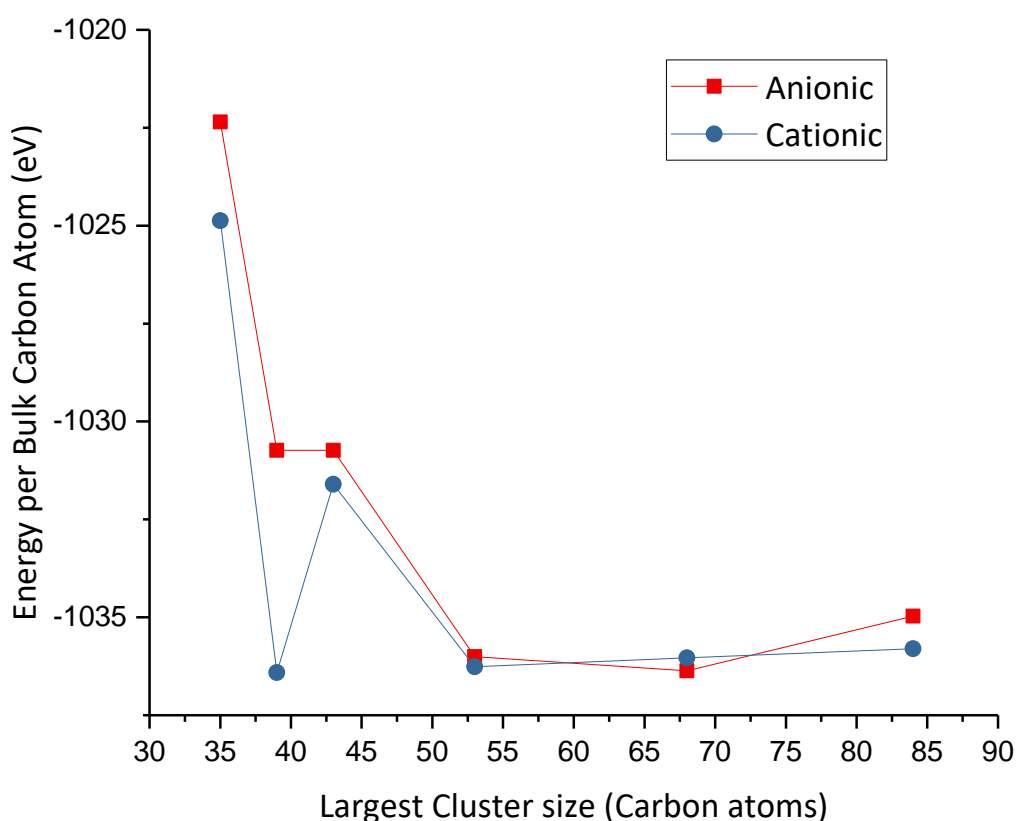


Figure 36: Energy per bulk carbon atom of the cationic and anionic clusters calculated by applying the hierarchical method to clusters ranging in size from 18-84 carbon atoms.

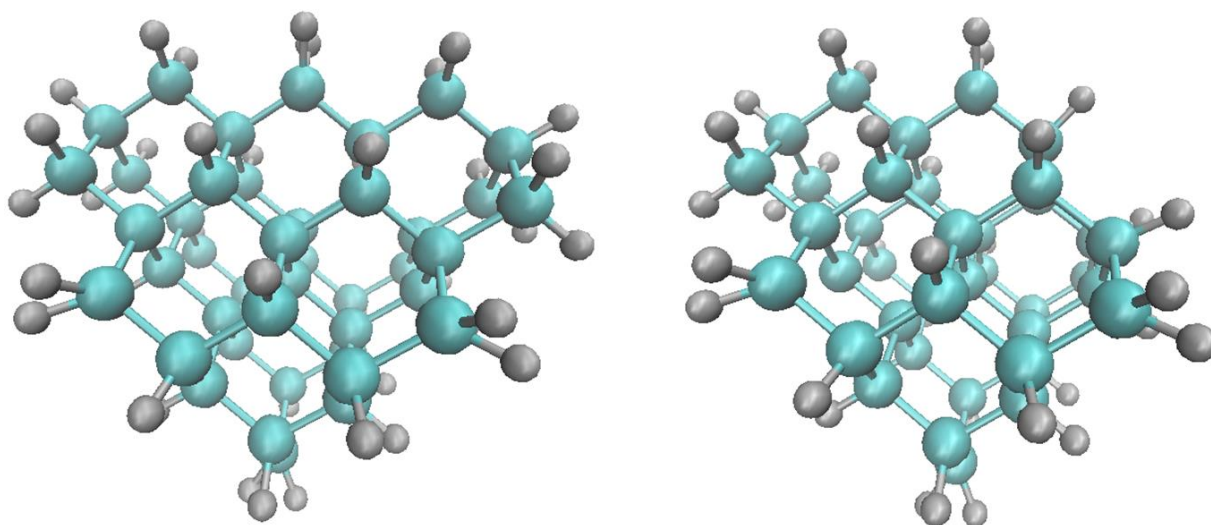


Figure 37: Systematic generation of the 39-carbon cluster (right) from the 43-carbon cluster (left) by removing the corner unit.

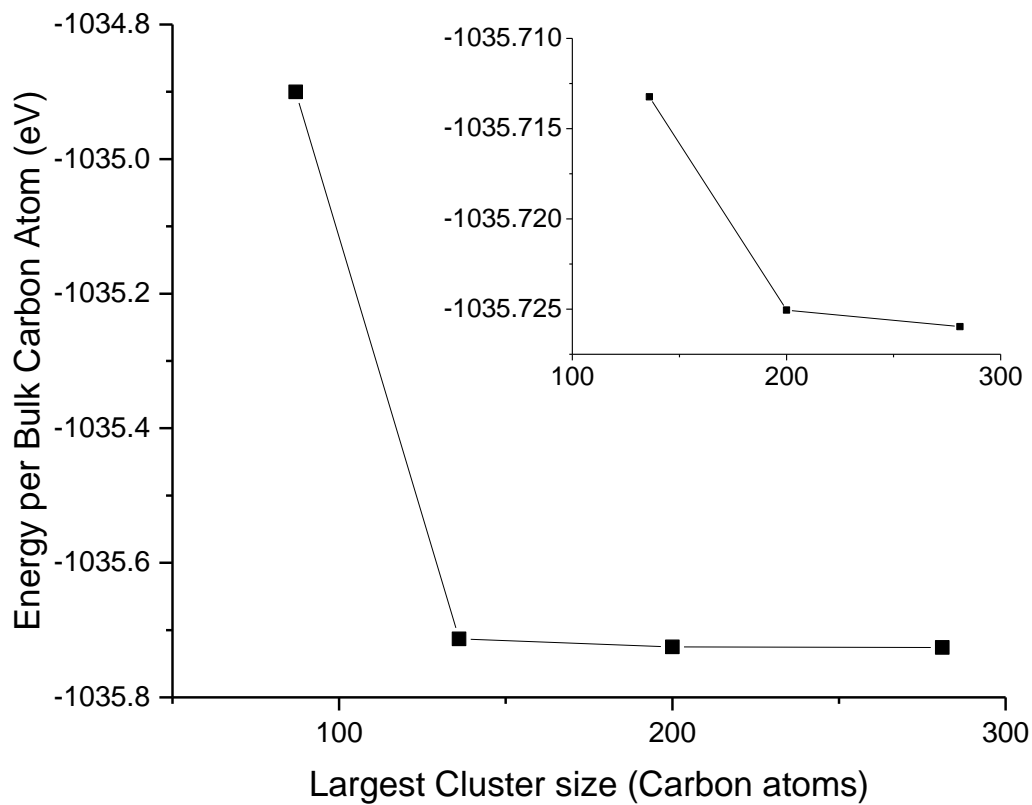


Figure 38: Energy per bulk carbon atom calculated using the hierarchical method with tetrahedral clusters ranging in size from 26 to 281 carbon atoms. The insert shows the last three points.

Total Number of Carbon Atoms	Total Number of Atoms	Number of Bulk Carbons	Number of Carbons with One Hydrogen	Number of Carbons with Two Hydrogens
26	57	7	7	12
51	103	17	16	18
87	163	35	28	24
136	240	62	44	30
200	336	100	64	36
281	453	151	88	42

Table 3: Details of the tetrahedral clusters built.

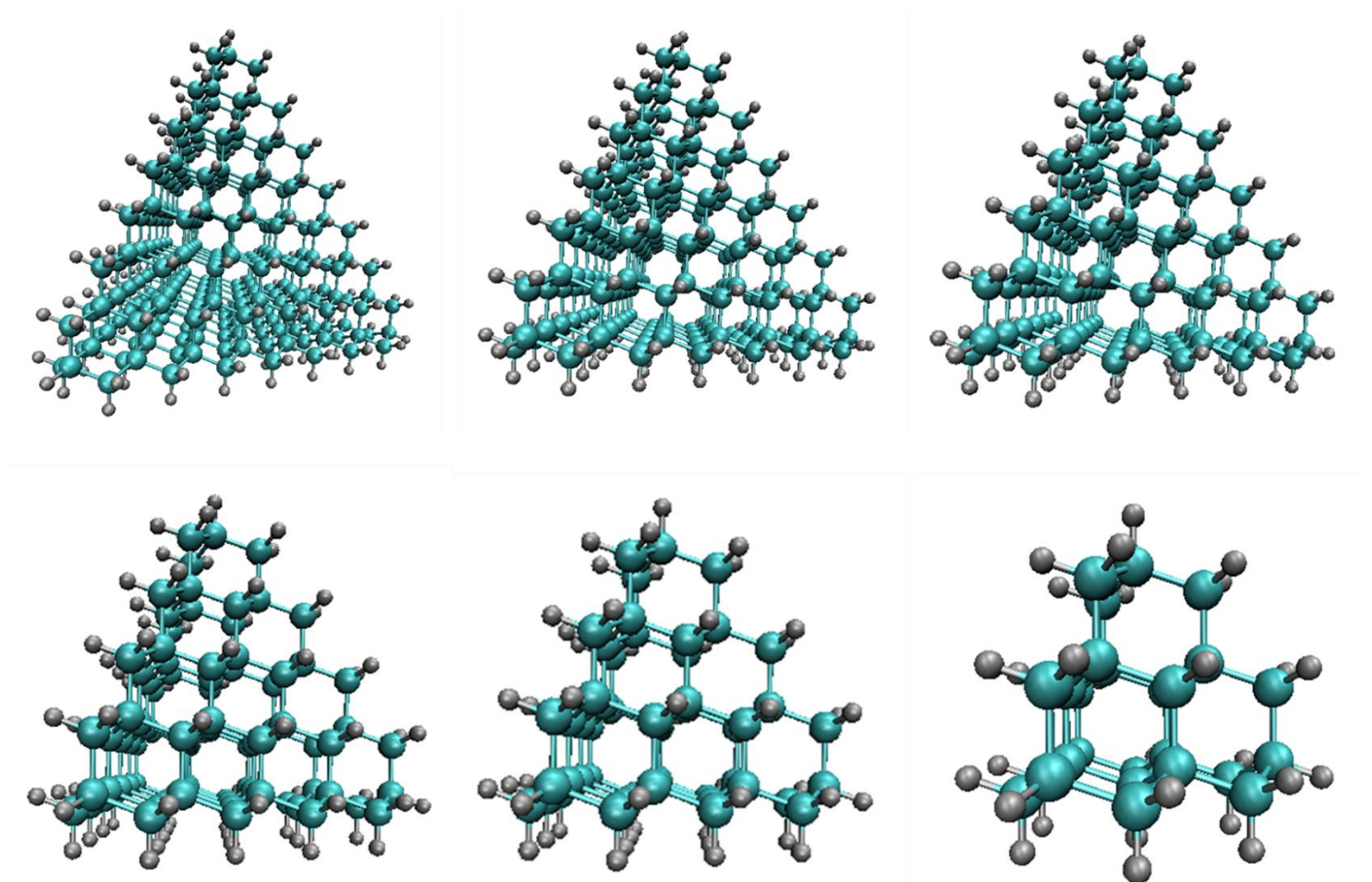


Figure 39: The tetrahedral clusters built by removing the bottommost plane of carbon atoms. These are (from left to right) are the 281-carbon cluster, 200-carbon cluster, 136-carbon cluster, 87-carbon cluster, 51-carbon cluster, and 26-carbon cluster.

4 Conclusions and Further Work

The experimental objective of this project was to fabricate and characterise an aluminium-oxygen-terminated diamond surface as a possible route to a low work function material. The fabrication was attempted by depositing thick films of aluminium onto oxygen-terminated polycrystalline diamond followed by a wet etch in hydrochloric acid. However, this was found to be unreliable and inconsistent, resulting in heterogeneous deposition. This was indicated by the visibly heterogeneous surface observed when using a short etching time of 10 min. This could be due to the nature of polycrystalline diamond having uneven topography as well as the different crystal planes having different chemistry, or it could be a product of the evaporation method as the equipment being used was not designed for such a thick deposition.

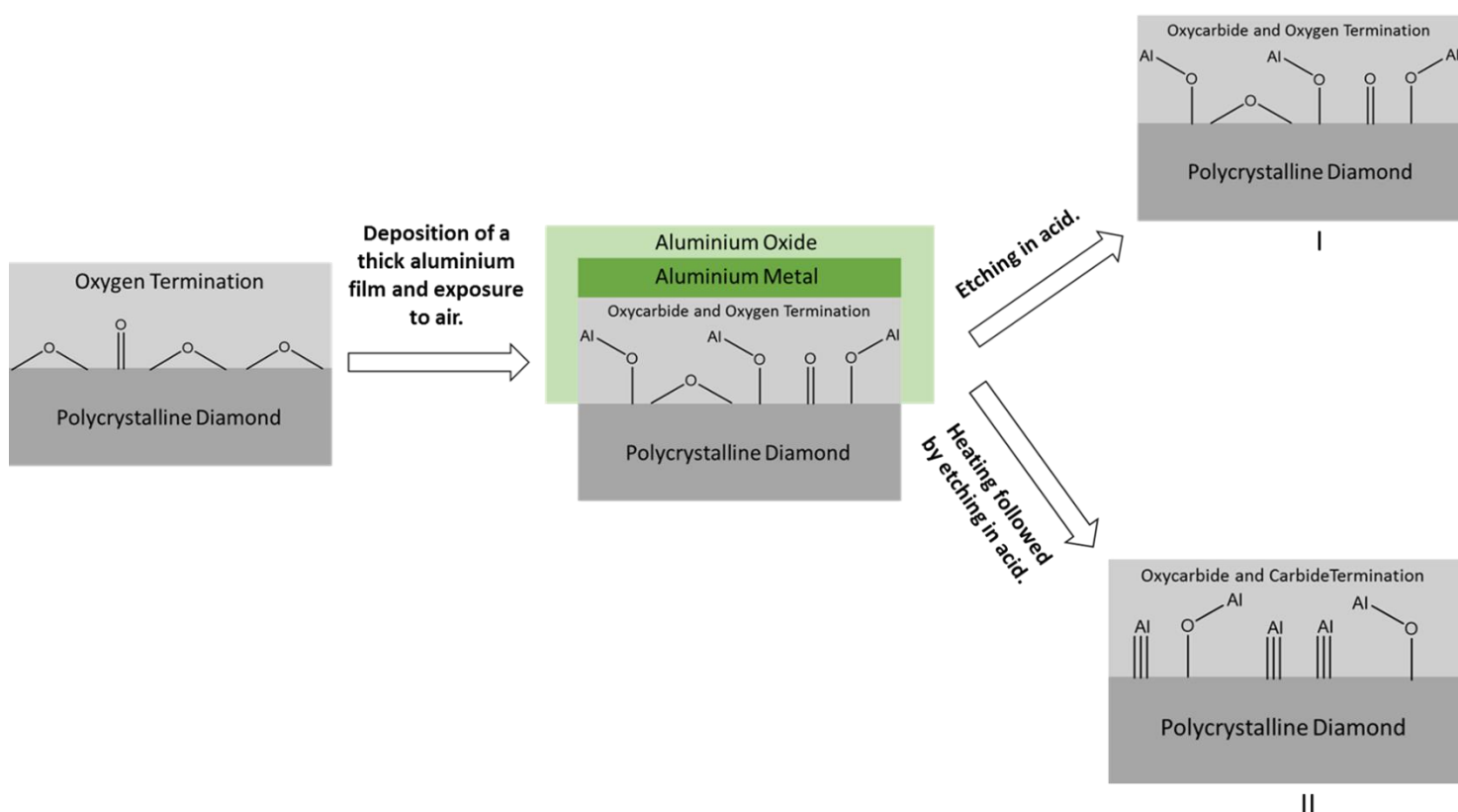


Figure 40: A cartoon of the proposed nature of the diamond-aluminium interface.

Some information was gleaned about the chemical nature of the diamond-aluminium interface using XPS, which showed that the etching procedure leaves aluminium bonded to the surface only as an oxycarbide (Figure 40 (I)). Such a structure has been shown by O'Donnell *et al.* to be optimal for lowering the work function of diamond in the case of lithium and magnesium coatings^{26,76}. However, no thermionic emission current was observed, indicating the material did not have a NEA and the aluminium had not lowered the work function sufficiently for thermionic emission to take place. This

might be because either aluminium lacks the capacity to induce a NEA, or there were only small quantities of aluminium present on the diamond surface. With regards the latter point, it seems unlikely that the harshness of the etching conditions was responsible for the small amounts of aluminium remaining, since 1.2M HCl would struggle to break the covalent linkage between the diamond surface and the aluminium. A more likely explanation is that there was a lack of bonding between aluminium and the oxygen-terminated diamond surface upon deposition.

The utility of heating prior to etching in order to increase the proportion of aluminium tightly bonded to the diamond surface did result in a larger quantity of aluminium being covalently bonded to the surface. However, it also changed the nature of the interaction, promoting carbide formation, by allowing the aluminium to either displace terminating oxygen atoms, or react with non-oxygenated diamond (Figure 40 (II)). Such bonding has been shown to be non-ideal for the lowering of work function and the formation of a NEA ^{26,76}.

A solution to many of these issues would be to deposit aluminium on smooth, single-crystal diamond using O'Donnell *et al's*. thin film method. Such a substrate removes the issues posed by the uneven topography of polycrystalline diamond, together with any effect the different chemistries of the different crystal planes may have on aluminium deposition and bonding. The thin-film method has a huge number of advantages over the thick-film method employed in this investigation. Firstly, sub-monolayer quantities of aluminium can be deposited and the thickness of the layer monitored *in situ*. Consequently, there is no necessity for a wet etch which can introduce further variability into the fabrication process. Secondly, the thin-film method allows for more controllable experimental conditions to be employed as the sample can be both fabricated and characterised within UHV. This would reduce the chance of contaminating the surface during deposition. It would also remove the necessity for degassing anneals, which employ elevated temperatures of around 300°C and could affect the nature of the diamond-aluminium interface. Unfortunately, fabrication of aluminium deposited diamond surfaces could not be carried out using the thin-film method during this project as the necessary equipment was not available for use.

In the future, if the thin-film method can be successfully applied to single-crystal diamonds, it would be informative to carry UPS. This can provide more information on the nature of adsorbate-substrate interactions and is one of the more reliable methods for detecting NEA, due to the presence of peaks which correspond to electrons being ejected from below the conduction band minimum ⁹⁵. Another analytical technique which may be of interest is total photoelectron yield spectroscopy which is a method for giving unequivocal evidence of a NEA ⁵⁰.

Finally, because the formation of the aluminium carbide could be indicative of incomplete oxygen termination, in the future it would be worthwhile to investigate the nature of the oxygen termination achieved. Since the geometry of the oxygen termination is known to affect the metal-surface interaction^{26,76} it would also be interesting to introduce different geometries of oxygen termination which can be formed using different methods of oxygenation *e.g.* ozonolysis.

With regards the computational objective of this project, it has proven very difficult to apply the hierarchical method to diamond. One of the main issues was trying to build clusters which are systematically related. This is partly due to the tetrahedral nature of diamond, but also the necessity for capping hydrogens which further complicates the building of diamond clusters. The capping hydrogens introduce a steric limitation in building the clusters, which prevents systematic growth because many algorithms generate clusters which are not chemically plausible. Once a systematic procedure for cluster building was developed, which resulted in chemically plausible clusters being formed, good convergence in the neutral energy per bulk atom was seen. However, this procedure resulted in a large growth in the number of atoms in each cluster. Each step up to a larger cluster results in roughly a 50% increase in the number of atoms and these clusters quickly become too large for the application of wavefunction theory.

Another issue, which has not been addressed in this work, is the term for the contribution per formula unit. Whilst this is straight forward to include for simple solids, such as lithium hydride and crystalline neon, it is unclear what this term should be when calculating the band gap for diamond. There is no single unit for diamond; the closest approximation would be a methane molecule. However, this unit is not present in any diamond structure and the band gap is not a molecular property. When applying the hierarchical method, this term was ignored, which could have had an enormous effect on the calculated results.

The next steps in this work would be to find a way of building smaller clusters which are systematically related and including the term for the contribution per formula unit in the calculations. In addition, calculations could also be performed using wavefunction theory, such as Moller-Plesent perturbation theory and coupled-cluster theory, which are more accurate but are more computationally demanding. Another avenue of research would be to look at the effect of different functionals on the DFT calculations.

5 References

- 1 Central Intelligence Agency, *The CIA World Factbook 2017*, Skyhorse Publishing, New York, 2016.
- 2 N. H. Batjes, *Eur. J. Soil Sci.*, 1996, **47**, 151–163.
- 3 P. M. Cox, R. a Betts, C. D. Jones, S. a Spall and I. J. Totterdell, *Nature*, 2000, **408**, 184–187.
- 4 E. A. Davidson and I. A. Janssens, *Nature*, 2006, **440**, 165–73.
- 5 K. Emanuel, *Nature*, 2005, **436**, 686–688.
- 6 P. J. Webster, G. J. Holland, J. A. Curry and H.-R. Chang, *Science*, 2005, **309**, 1844–1846.
- 7 J. G. Ayres, R. Maynard and R. Richards, *Lancet*, 2002, **360**, 1233–1242.
- 8 C. A. Pope III, R. T. Burnett, M. J. Thun, E. E. Calle, D. Krewski and G. D. Thurston, *J. Am. Med. Assoc.*, 2002, **287**, 1132–1141.
- 9 D. W. Dockery, C. Arden Pope III, X. Xu, J. D. Spengler, J. H. Ware, M. E. Fay, B. G. Ferris and F. E. Speizer, *N. Engl. J. Med.*, 1993, **329**, 1753–1759.
- 10 C. J. Vörösmarty, C. J. Vo and P. Green, *Science*, 2009, **289**, 284–288.
- 11 S. Kazim, M. K. Nazeeruddin, M. Grätzel and S. Ahmad, *Angew. Chemie - Int. Ed.*, 2014, **53**, 2812–2824.
- 12 M. Liang and J. Chen, *Arylamine organic dyes for dye-sensitized solar cells.*, 2013, vol. 42.
- 13 A. Mishra and P. Bäuerle, *Angew. Chemie - Int. Ed.*, 2012, **51**, 2020–2067.
- 14 Y. Lin, Y. Li and X. Zhan, *Chem. Soc. Rev.*, 2012, **41**, 4245.
- 15 E. P. Gyftopoulos and G. N. Hatsopoulos, *Thermionic Energy Conversion I*, The MIT Press, Cambridge, Massachusetts, 1st edn., 1974.
- 16 K. A. A. Khalid, T. J. Leong and K. Mohamed, *IEEE Trans. Electron Devices*, 2016, **63**, 2231–2241.
- 17 S. Dushman, *Phys. Rev.*, 1923, **21**, 623–636.
- 18 F. A. M. Koeck, R. J. Nemanich, Y. Balasubramaniam, K. Haenen and J. Sharp, *Diam. Relat. Mater.*, 2011, **20**, 1229–1233.
- 19 X. Chang, Q. Wu, I. Ben-zvi, A. Burrill, J. Kewisch, T. Rao, J. Smedley, E. Wang, E. M. Muller, R. Busby and D. Dimitrov, *Phys. Rev. Lett.*, 2010, **105**, 2–5.
- 20 D. A. G. Deacon, L. R. Elias, J. M. J. Madey, G. J. Ramian, H. A. Schwettman and T. I. Smith, *Phys. Rev. B - Condens. Matter Mater. Phys.*, 1977, **38**, 892–894.
- 21 G. R. Neil, C. L. Bohn, S. V. Benson, G. Biallas, D. Douglas, H. F. Dylla, R. Evans, J. Fugitt, A. Grippo, J. Gubeli, R. Hill, K. Jordan, R. Li, L. Merminga, P. Piot, J. Preble, M. Shinn, T. Siggins, R. Walker and B. Yunn, *Phys. Rev. Lett.*, 2000, **84**, 662–665.
- 22 M. Tigner, *Nuovo Cim. Ser. 10*, 1965, **37**, 1228–1231.
- 23 S. M. Gruner, D. Bilderback, I. Bazarov, K. Finkelstein, G. Krafft, L. Merminga, H. Padamsee, Q. Shen, C. Sinclair and M. Tigner, *Rev. Sci. Instrum.*, 2002, **73**, 1402–1406.
- 24 J. E. Field, *The Properties of Natural and Synthetic Diamond*, 1992.

- 25 P. W. May, *Science*, 2008, **319**, 1490–1491.
- 26 K. M. O. Donnell, T. L. Martin, N. A. Fox and D. Cherns, *Phys. Rev. B*, 2010, **82**, 115303.
- 27 G. Glockler, *J. Chem. Phys.*, 1953, **21**, 1242–1248.
- 28 R. Abbaschian, H. Zhu and C. Clarke, *Diam. Relat. Mater.*, 2005, **14**, 1916–1919.
- 29 A. Onodera, K. Suito and Y. Morigami, *Proc. Jpn. Acad.*, 1992, **68**, 167–171.
- 30 K. Suzuki, A. Sawabe, H. Yasuda and T. Inuzuka, *Appl. Phys. Lett.*, 1987, **50**, 728–729.
- 31 M. N. R. Ashfold, P. W. May, C. A. Rego and N. M. Everitt, *Chem. Soc. Rev.*, 1994, **23**, 21–30.
- 32 P. W. May, N. Ali, A. Ochsner and W. Ahmed, in *Carbon Based Nanomaterials*, 2010, pp. 147–175.
- 33 W. Ahmed, W. Ahmed, C. A. Rego, R. Cherry, A. Afzal, N. Ali and I. U. Hassan, *Vacuum*, 2000, **56**, 153–158.
- 34 I. Nasioka, V. Strelchuk, M. Boyko, V. Voevodin, A. Vierovkin, A. Rybka, V. Kutniy, S. Dudnik, V. Gritsina, O. Opalev and V. Strel’Nitskij, *Sensors Actuators, A Phys.*, 2015, **223**, 18–23.
- 35 S. Matsumoto and M. Tsutsumi, *J. Mater. Sci.*, 1982, **17**, 3106–3112.
- 36 S. C. Eaton and M. K. Sunkara, *Diam. Relat. Mater.*, 2000, 1320–1326.
- 37 Y. A. Mankelevich and P. W. May, *Diam. Relat. Mater.*, 2008, **17**, 1021–1028.
- 38 S. J. Harris, *Appl. Phys. Lett.*, 1990, **56**, 2298–2300.
- 39 D. Petrini and K. Larsson, *J. Phys. Chem. C*, 2007, **111**, 795–801.
- 40 K. C. Pandey, *Phys. Rev. B*, 1982, **25**, 4338–4341.
- 41 N. Fukimori, H. Nakahata and T. Imai, *Jpn. J. Appl. Phys.*, 1990, **29**, 824–827.
- 42 R. Kalish, *Diam. Relat. Mater.*, 2001, **10**, 1749–1755.
- 43 N. W. Ashcroft and N. D. Mermin, *Solid State Physics*, Holt, Rinehart and Winston, 1st edn., 1976.
- 44 C. E. Nebel, D. Shin, B. Rezek, N. Tokuda, H. Uetsuke and H. Watanabe, *J. R. Soc. Interface*, 2007, **4**, 439–461.
- 45 K. Takahashi, M. Tanga, O. Takai and H. Okamura, *Diam. Relat. Mater.*, 2003, **12**, 572–576.
- 46 S. Szunerits and R. Boukherroub, *J. Solid State Electrochem.*, 2008, **12**, 1205–1218.
- 47 S. J. Sque, R. Jones and P. R. Briddon, *Phys. Rev. B - Condens. Matter Mater. Phys.*, 2006, **73**, 1–15.
- 48 M. Wang, N. Simon, C. Decorse-Pascanut, M. Bouttemy, A. Etcheberry, M. Li, R. Boukherroub and S. Szunerits, *Electrochim. Acta*, 2009, **54**, 5818–5824.
- 49 T. Ando, K. Yamamoto, M. Ishii, M. Kamo and Y. Sato, *J. Chem. Soc. Faraday Trans.*, 1993, **89**, 3635.
- 50 K. M. O’Donnell, T. L. Martin, M. T. Edmonds, A. Tadich, L. Thomsen, J. Ristein, C. I. Pakes, N. A. Fox and L. Ley, *Phys. Status Solidi Appl. Mater. Sci.*, 2014, **211**, 2209–2222.
- 51 S. Petrick and C. Benndorf, *Diam. Relat. Mater.*, 2001, **10**, 519–525.

- 52 F. Maier, J. Ristein and L. Ley, *Phys. Rev. B*, 2001, **64**, 165411.
- 53 J. B. Cui, J. Ristein and L. Ley, *Phys. Rev. Lett.*, 1998, **81**, 429–432.
- 54 C. Bandis and B. B. Pate, *Phys. Rev. Lett.*, 1995, **74**, 777–780.
- 55 F. J. Himpsie, J. A. Knapp, J. A. Van Vechten and D. E. Eastman, *Phys. Rev. B*, 1979, **20**, 624–627.
- 56 D. Zhu, L. Zhang, R. E. Ruther and R. J. Hamers, *Nat. Mater.*, 2013, **12**, 836–841.
- 57 K. M. O. Donnell, M. T. Edmonds, J. Ristein, A. Tadich, L. Thomsen, Q. Wu, C. I. Pakes and L. Ley, *Adv. Funct. Mater.*, 2013, **23**, 5608–5614.
- 58 A. K. Tiwari, J. P. Goss, P. R. Briddon, A. B. Horsfall, N. G. Wright, R. Jones and M. J. Rayson, *EPL*, 2014, **108**, 46005.
- 59 P. K. Baumann and R. J. Nemanich, *Phys. Rev. B*, 1998, **58**, 1643–1654.
- 60 J. S. Foord, L. C. Hian and R. B. Jackman, *Diam. Relat. Mater.*, 2001, **10**, 710–714.
- 61 J. S. Foord, J. Wang, C. Hian and M. Hiramatsu, *Phys. status solidi a*, 2001, **186**, 227–233.
- 62 K. M. O. Donnell, M. T. Edmonds, A. Tadich, L. Thomsen, A. Stacey, A. Schenk, C. I. Pakes and L. Ley, *Phys. Rev. B*, 2015, **92**, 35303-1-35303–1.
- 63 A. K. Tiwari, J. P. Goss, P. R. Briddon, N. G. Wright, A. B. Horsfall and M. J. Rayson, *Phys. status solidi a*, 2012, **209**, 1697–1702.
- 64 P. K. Baumann and R. J. Nemanich, *Appl. Surf. Sci.*, 1996, **105**, 267–273.
- 65 J. Van Der Weide and R. J. Nemanich, *Phys. Rev. B*, 1994, **49**, 13629–13637.
- 66 J. Van Der Weide and R. J. Nemanich, *J. Vac. Sci. Technol. B*, 1992, **10**, 1940–1943.
- 67 P. K. Baumann and R. J. Nemanich, *J. Appl. Phys.*, 1998, **83**, 2072.
- 68 K. W. Wong, Y. M. Wang, S. T. Lee and R. W. M. Kwok, *Diam. Relat. Mater.*, 1999, **8**, 1885–1890.
- 69 K. W. Wong, Y. M. Wang and S. T. Lee, *Appl. Surf. Sci.*, 1999, **140**, 144–149.
- 70 K. P. Loh, J. S. Foord, R. G. Egdell and R. B. Jackman, *Diam. Relat. Mater.*, 1997, **6**, 874–878.
- 71 M. W. Geis, J. C. Twichell, J. Macaulay and K. Okano, *Appl. Phys. Lett.*, 1995, **67**, 1328.
- 72 J. Van Der Weide and R. J. Nemanich, *Phys. Rev. B*, 1994, **49**, 13629–13637.
- 73 F. H. Jones, A. B. Molloy, K. P. Loh, J. S. Foord and R. B. Jackman, *Diam. Relat. Mater.*, 1998, **7**, 651–655.
- 74 M. W. Geis, J. C. Twichell, J. Macaulay and K. Okano, *Appl. Phys. Lett.*, 1995, **67**, 1328–1330.
- 75 M. . Hossain, T. Kubo, T. Aruga, N. Takagi, T. Tsuno, N. Fujimori and M. Nishijima, *Diam. Relat. Mater.*, 2000, **9**, 162–169.
- 76 K. M. O’Donnell, T. L. Martin and N. L. Allan, *Chem. Mater.*, 2015, **27**, 1306–1315.
- 77 W. Koch and M. C. Holthausen, *A Chemist’s Guide to Density Functional Theory*, 2001, vol. 3.
- 78 B. Paulus, *Phys. Rep.*, 2006, **428**, 1–52.
- 79 S. J. Nolan, M. J. Gillan, D. Alfè, N. L. Allan and F. R. Manby, *Phys. Rev. B - Condens. Matter Mater. Phys.*, 2009, **80**, 1–7.

- 80 F. R. Manby, D. Alf and M. J. Gillan, *Phys. Chem. Chem. Phys.*, 2006, **8**, 5178.
- 81 S. J. Nolan, P. J. Bygrave, N. L. Allan and F. R. Manby, *J. Phys. Condens. Matter*, 2010, **22**, 74201.
- 82 M. Z. Othman, PhD thesis, University of Bristol, 2014.
- 83 S. C. Halliwell, PhD thesis, University of Bristol, 2017.
- 84 R. Irlam, MSc thesis, University of Bristol, 2014.
- 85 T. R. Gilson and P. J. Hendra, *Laser Ram Spectroscopy*, Wiley-Interscience, 1st edn., 1970.
- 86 G. Attard and C. Barnes, *Surfaces*, Oxford Univeristy Press, Oxford, 1998.
- 87 S. Prawer and R. J. Nemanich, *Philos. Trans. A. Math. Phys. Eng. Sci.*, 2004, **362**, 2537–2565.
- 88 P. W. May, J. a. Smith and K. N. Rosser, *Diam. Relat. Mater.*, 2008, **17**, 199–203.
- 89 P. W. May, *Philos. Trans. R. Soc. A Math. Phys. Eng. Sci.*, 2000, **358**, 473–495.
- 90 R. G. Forbes, *Solid. State. Electron.*, 2001, **45**, 779–808.
- 91 A. Fernandez, J. P. Espinos, D. Leinen, A. R. Gonz??lez??Elipe and J. M. Sanz, *Surf. Interface Anal.*, 1994, **22**, 111–114.
- 92 T. L. Barr, *Practical Surface Analysis vol. 1*, Wiley, New York, 1990.
- 93 B. Maruyama, 2017, **6**, 1131–1134.
- 94 P. M. A. Sherwood, *Surf. Sci. Spectra*, 1998, **5**, 1–3.
- 95 L. Diederich, O. M. Kuttel, P. Aebi, E. Maillard-Schaller, R. Fasel and L. Schlapbach, *Diam. Relat. Mater.*, 1998, **7**, 660–665.
- 96 E. Staryga, K. Fabisiak, M. Dłużniewski and G. Bąk, *Mater. Sci.*, 2012, **30**, 390–397.
- 97 Turbmole user's manual, http://www.turbomole-gmbh.com/manuals/version_5_10/DOK_HTML/node54.html (accessed 20/4/2017)
- 98 S. J. Binnie, S. J. Nolan, N. D. Drummond, D. Alf??, N. L. Allan, F. R. Manby and M. J. Gillan, *Phys. Rev. B - Condens. Matter Mater. Phys.*, 2010, **82**, 1–10.
- 99 C. D. Clark, P. J. Dean and P. V. Harris, *Proc. R. Soc. London*, 1964, **277**, 312–329.